A study of solar energetic particle events of 1997–2006: Their composition and associations

H. V. Cane,[1,2] I. G. Richardson,[1,3] and T. T. von Rosenvinge[1]

Received 29 August 2009; revised 29 January 2010; accepted 26 February 2010; published 4 August 2010.

[1] We examined the properties and associations of 280 solar proton events that extended above 25 MeV and occurred in the years 1997–2006. The properties include early peak intensities of five species over several energy ranges and the intensity-time profiles. Solar event associations were made for as many events as possible. The solar parameters determined include coronal mass ejection and flare properties and radio emissions from a wavelength range of meters to kilometers. The events were divided into five representative types based on the relative abundances and particle profiles to more easily illustrate how particle characteristics vary with the solar parameters. We find a continuum of event properties with no indication of specific parameters that clearly separate out groups of events. There is, however, a reasonable separation of events based on the timing of the associated type III emissions relative to the H α flare. Type III bursts indicate the presence of flare particles that escape to the interplanetary medium. The least intense, relatively short-lived, proton events that are electron-rich (and generally Fe-rich and He-rich) have associated type III bursts that occur at the start of the flare (i.e., in the impulsive phase), indicating rapid acceleration and escape of particles. In the largest events the type III emissions occur after the impulsive phase. It is likely that this late acceleration and/or release of particles results in a composition different from that of impulsive acceleration and release. A scenario in which concomitant flare processes contribute particles in the majority of solar energetic particle events is consistent with the observations.

Citation: Cane, H. V., I. G. Richardson, and T. T. von Rosenvinge (2010), A study of solar energetic particle events of 1997–2006: Their composition and associations, *J. Geophys. Res.*, *115*, A08101, doi:10.1029/2009JA014848.

1. Introduction

[2] We examined the properties, associations, and abundance variations of 280 >25 MeV proton increases seen by near-Earth spacecraft in the years 1997–2006. A motivation for this study is to provide a comprehensive catalog of the properties of >25 MeV proton events with a wide range of intensities during most of solar cycle 23. Many other studies just consider the large events in the NOAA proton event list that have high integral intensities for protons at energies above 10 MeV and consequently are biased toward events with many locally shock-accelerated particles. Here our specific interest is in the properties of the particles in the early stages of solar energetic particle (SEP) events, which may provide evidence about acceleration processes occurring close to the Sun.

[3] Our main conclusion is that we find a continuum of event properties that does not support the simplest "two-class" picture of SEP events, with flares producing the particles in one (the impulsive) class and only shocks accelerating the particles in the other (the gradual class) [*Reames*, 1999]. In this picture [*Reames*, 1988; *Reames and Ng*, 2004], large gradual events have Fe/O ~ 0.1, similar to the value in the ambient corona and solar wind, and are well associated with interplanetary shocks and associated particle enhancements at 1 AU. In contrast, impulsive events are Fe–rich (i.e., they have Fe/O ratios greater than those of the corona and solar wind), are not associated with shocks, and are also ^{3}He–rich (^{3}He/^{4}He ratios 100–1000 times those in the solar wind). These enhanced abundances can be understood in terms of an acceleration process in flares in which particles interact with resonant waves [*Reames*, 1999]. These events supposedly lack coronal mass ejections (CMEs) and type II radio bursts (related to shocks) but include type III bursts (caused by flare electron beams). Finally, gradual events should be seen from anywhere on the solar disk (and beyond), as expected from large-scale shock acceleration, whereas impulsive events would originate in a much more limited longitude range a few tens of degrees wide.

[4] Instead, our observations add to the evidence, largely obtained with improved instrumentation in cycle 23, that

[1]NASA Goddard Space Flight Center, Greenbelt, Maryland, USA.
[2]Also at School of Mathematics and Physics, University of Tasmania, Hobart, Tasmania, Australia.
[3]Also at CRESST and Department of Astronomy, University of Maryland, College Park, Maryland, USA.

Copyright 2010 by the American Geophysical Union.
0148-0227/10/2009JA014848

this simple two-class picture does not match the diversity of observed particle event properties. Such evidence includes the following:

[5] 1. Abundance enhancements similar to those in impulsive events are seen in some large events [*Cohen et al.*, 1999, *Mason et al.*, 1999; see also *McGuire et al.*, 1986, and references therein], at some energies, and in the early stages of the events.

[6] 2. Some impulsive events are associated with CMEs [*Kahler*, 2001; *Nitta et al.*, 2006].

[7] 3. Gradual events are also associated with type III bursts, although these are long-lived and extend, or start, beyond the flare impulsive phase [*Cane et al.*, 2002].

[8] We suggest that our observations are consistent with proposals [*Kocharov and Torsti*, 2002; *Kallenrode*, 2003; *Cane et al.*, 2003, 2006; *Klein and Posner*, 2005] that both flare and shock acceleration can contribute in the largest SEP events. Note that we use the term "flare" broadly and to mean particle acceleration involving some sort of reconnection and, in particular, including widespread magnetic reconfiguring in the aftermath of a CME [see also *Maia et al.*, 2007].

2. Data Sets and Event Associations

[9] The events discussed in this paper compose a subset of the ~340 proton events observed at energies above ~25 MeV in the years 1997–2006. We list in Table 1 those 280 SEP events that had a peak proton intensity in the ~20–30 MeV range above 2×10^{-4} particles/(cm^2 sr s MeV) and that were not compromised by data gaps and other events. Proton and helium data were obtained from the Goddard Space Flight Center (GSFC) experiment on IMP 8 and the University of Turku ERNE instrument on the Solar and Heliospheric Observatory (SOHO). In a few cases we also used the GSFC EPACT instrument on Wind. The first three columns in Table 1 provide the onset times of the protons to the nearest hour. The date is that of the associated flare so that if the particles rise on the following day the hour can be >23. Column 4 gives an estimate of the highest energy at which a proton increase could be discerned. In some cases this value was obtained from the GOES HEPAD instrument. A value of 900 MeV indicates that an event was seen on Earth by neutron monitors. The listed ~25 MeV proton intensity in column 5 is the maximum reached within the first ~12 h after the solar event. This value is used because we are interested in the early stages of events when signatures of the acceleration processes near the Sun should be most apparent. This is not necessarily the peak intensity of an event, which often occurs near passage of the related interplanetary shock at the spacecraft. We flagged the minority of events for which the intensities rise slowly over more than a day by placing a less than symbol before the onset time.

[10] For each event we examined additional energetic particle data sets. Electron data were obtained from the University of Kiel EPHIN experiment on SOHO or the John Hopkins University Applied Physics Laboratory Electron, Proton, and Alpha Monitor (EPAM) experiment on ACE when SOHO was not operating. Fe and O intensities over the range 0.1–~70 MeV/nucleon were examined using the ULEIS and SIS experiments on ACE. We did not examine ^{3}He intensities because accurate determination of these intensities requires a careful analysis of original data rather than using web-based data sets. Furthermore, the threshold for ^{3}He in the SIS instrument is too high for many events.

[11] Columns 6–13 of Table 1 give details of the associated solar phenomena. Reliable associations of the SEP increases with solar events were facilitated by using radio data. We identified the type III radio bursts extending to very low frequencies observed by Wind/WAVES [*Cane et al.*, 2002] that had solar onset times close to the onset times of the energetic electrons in the SEP events. The approximate times of these emissions at 14 MHz are given in the table. We also previously demonstrated that the rate at which the radio burst drifts to the lowest frequencies indicates how well the event is magnetically connected to near Earth [*Cane and Erickson*, 2003]. This rate is also matched to the particle intensity rise rate such that particle events that have rapid increases are associated with radio bursts that drift rapidly [*Cane and Erickson*, 2003]. Radio data can also indicate events that originated behind the limb of the Sun. In such cases, high-frequency emissions are absent because of occultation and the type III bursts start near 1 MHz rather than above 14 MHz, the highest frequency for the WAVES experiment. In such events there were no reported H α flares but CMEs were observed above the limb. For these events, only an approximate time for the radio emission is listed.

[12] In addition to type III emissions, many of the events had associated type II emissions. For meter-wavelength observations the original data were examined rather than relying on reports in Solar Geophysical Data (SGD) since *Cane et al.* [2002] emphasized that metric type II burst reports are often unreliable. The intensity class given in SGD is listed in the table for when type II activity was deemed to be present. An entry of zero indicates that metric type II activity was absent. Emissions at longer wavelengths (originating in the interplanetary medium) were determined from the WAVES data. These were categorized according to the frequency extent and duration by examining the dynamic spectra and lists available at http://cdaw.gsfc.nasa.gov/CME_list/radio/waves_type2.html.

[13] The parameters of the associated flares (soft X-ray peak intensity and risetime; H α location and duration) obtained from reports in SGD are given in Table 1. When an event was behind the limb but had an associated soft X-ray event the location was presumed to be <30° behind the limb. For some of the behind-the-limb events, the longitude was estimated from the time since a probably associated active region went over the limb. For the remaining behind-the-limb events, the longitudes were assigned 140°.

[14] Associated CMEs were identified using the Catholic University of America (CUA) Large Angle and Spectrometric Coronagraph (LASCO) catalog [*Yashiro et al.*, 2004]. CMEs were typically first observed about 30 min after the onset of the type III bursts. When coronagraph observations were available, all of the SEP events could be associated with a CME despite the fact that some of the proton increases were very minor. (This was also the case for the vast majority of the other ~60 >25 MeV proton events that were too small to be included in this study.) The CME sky-plane speeds given in Table 1, determined from a linear fit to the height-versus-time profiles, were taken from the CUA catalog. [One exception, the event of 10 November 2004, had an unusually high speed of 3387 km/s in the CUA catalog. However, the LASCO observer measured a maximum speed of only

Table 1. SEP Events (1997–1999)

	Proton Event						Flare Event				CME				
	Time[a]		E[b]		Type III Time[d]	Type II	Start	Rise	H α	X-ray	First Obs.	Size[g]	Speed	Shock Speed[h]	
Year	Date(s)	Hour	(MeV)	Intensity[c]	(UT)	Int.[e]	(UT)	(min)	Position	Peak[f]	(UT)	(deg)	(km/s)	(km/s)	Group[i]
1997	1 Apr	16	50	0.001	1345–1355	3	1325	23	25S, 16E	M2	1518	40	312	···	dg
	7 Apr	15	70	0.005	1355–1440	3	1350	17	28S, 19E	C7	1427	80	878	550	dg
	12 May	06	80	0.009	0455–0510	3	0442	13	21N, 7W	C1	0630	360	464	600	dg
	21 May	21	70	0.001	2010–2015	3	2003	12	05N, 12W	M1	2100	30	296	380	dg
	25 Jul	21	40	0.003	2015–2025	3	2017	17	16N, 54W	C5	2101	50	611	···	dg
	24 Sep	04	120	0.003	0250–0300	3	0243	9	31S, 19E	M6	0300	70	532	···	dg
	7 Oct	14	50	0.003	~1320	2	···	···	S, 120W	···	1330	90	1271	430	dg
	21 Oct	20	45	0.0004	1740–1750	0	1700	54	16N, 07E	C3	1803	360	523	ps	dg
	3 Nov	11	40	0.002	1025–1030	3	1018	11	17S, 22W	M4	1111	100	352	···	dg
	4 Nov	07	500	0.9	0555–0615	3	0552	6	14S, 33W	X2	0610	110	785	640	2
	6 Nov	12	900	4.3	1150–1215	0	1149	6	18S, 63W	X9	1210	115	1556	500	2
	13 Nov	23	70	0.016	2115–2120	0	···	···	N, 110W	···	2225	180	546	···	1
	14 Nov	15	60	0.008	~1300	0	···	···	N, 120W	···	1336	140	702	···	dg
	6 Dec	17	30	0.0007	~1240	0	1059	270	47N, 13W	B7	1027	130	397	460	dg
1998	26 Jan	23	50	0.002	2235–2240	3	2219	16	17S, 55W	C5	2327	40	399	PS	1
	20 Apr	12	380	7.7	~1000	2	0938	43	S, 90W	M1	1007	150	1863	520	3
	29 Apr	<24	70	0.009	1615–1650	N	1606	31	18S, 20E	M7	1658	90	1374	780	5
	2 May	14	900	1.1	1335–1400	0	1331	11	15S, 15W	X1	1406	130	938	1120	2
	6 May	08	500	1.4	0800–0830	3	0758	11	11S, 65W	X3	0829	90	1099	PS	2
	9 May	05	120	0.08	0325–0350	3	0304	37	S, 100W	M8	0335	100	2331	···	2
	14 May	06	30	0.0004	0320–0325	N	···	···	S, W120	···	0355	40	351	ps	1
	27 May	15	50	0.001	1315–1330	0	1313	67	21S, 83W	C8	1345	90	878	PS	1
	30 May	25	70	0.001	2250–2255	2	···	···	S, 120W	···	2328	30	594	···	1
	4 Jun	14	40	0.0004	~0200	N	···	···	S, 120W	···	0204	110	1802	···	···
	16 Jun	21	70	0.01	~1810	1	1803	39	S, 115W	M1	1827	100	1484	PS	···
	18 Aug	24	70	0.002	2215–2220	3	2210	9	33N, 87E	X5	dg	dg	dg	PS	···
	19 Aug	23	120	0.008	2145–2155	3	2135	10	32N, 75E	X4	dg	dg	dg	PS	···
	24 Aug	23	900	1.6	2205–2230	3	2150	22	35N, 09E	X1	dg	dg	dg	1260	2
	6 Sep	07	75	0.008	~0500	0	0454	4	21S, 36W	C1	dg	dg	dg	···	1
	9 Sep	06	50	0.003	0455–0500	2	0452	6	21S, 75W	M2	dg	dg	dg	···	1
	20 Sep	<27	70	0.0003	0235–0250	3	0233	18	22N, 62E	M2	dg	dg	dg	···	···
	23 Sep	<10	120	0.009	0700–0715	3	0640	33	19N, 09E	M7	dg	dg	dg	1020	5
	27 Sep	09	50	0.001	0805–0810	0	0806	7	21N, 48W	C3	dg	dg	dg	···	1
	30 Sep	14	300	6.7	1320–1350	N	1304	44	19N, 85W	M3	dg	dg	dg	1010	2
	18 Oct	22	120	0.022	2105–2110	N	···	···	N, 120W	···	dg	dg	dg	···	1
	5 Nov	<22	60	0.0006	···	N	1900	55	26N, 18W	M9	2044	60	1118	730	5
	14 Nov	06	400	2.28	0500–0535	3	···	···	N, 120W	···	dg	dg	dg	···	2
	22 Nov	08	200	0.04	0640–0645	3	0630	12	27S, 82W	X4	dg	dg	dg	···	···
	24 Nov	03	120	0.011	0215–0220	3	0207	13	S, 108W	X1	0230	110	1798	···	1
	17 Dec	11	25	0.0003	0745–0750	3	0740	5	27S, 46W	M3	0830	dg	302	···	1
1999	3 Jan	16	30	0.0005	1450–1520	N	1449	25	23S, 49W	C6	dg	dg	dg	···	3
	6 Jan	25	30	0.0006	2400–2410	3	2354	12	S, 95W	C8	dg	dg	dg	···	···
	20 Jan	21	120	0.02	1905–1955	N	1906	58	S, 95E	M5	dg	dg	dg	PS	5
	16 Feb	06	70	0.001	0300–0320	2	0249	23	23S, 14W	M2	dg	dg	dg	870	···
	24 Apr	15	70	0.1	1300–1340	N	···	···	S, 120W	···	1331	120	1495	···	3
	3 May	<20	50	0.0001	0540–0615	2	0536	26	15N, 32E	M4	0606	110	1584	720	5
	9 May	19	90	0.02	1800–1805	N	1753	14	N, 95W	M8	1827	40	615	···	···
	27 May	11	150	0.06	1045–1110	N	···	···	S, 120W	···	1106	120	1691	···	3
	1 Jun	20	200	0.29	1845–1910	N	···	···	N, 120W	···	1937	180	1772	···	2
	4 Jun	08	120	0.29	0655–0730	2	0652	11	17N, 69W	M4	0726	80	2221	···	2
	11 Jun	01	150	0.042	~0040	3	···	···	N, 120W	···	0126	50	719	···	···
	18 Jun	18	30	0.001	1635–1640	N	1638	19	N, 120W	C6	dg	dg	dg	···	1
	27 Jun	11	60	0.002	0835–0840	2	0834	10	22N, 26W	X1	0906	40	903	PS	1
	29 Jun	<12	80	0.0006	0455–0515	2	0501	9	18N, 07E	M1	0554	360	589	ps	···
	25 Jul	20	70	0.0008	~1325	1	1308	30	N, 95W	M2	1331	90	1389	PS	···
	31 Jul	12	30	0.0006	~1150	N	1100	?	25N, 31E	C4	1126	150	1079	···	···
	28 Aug	20	70	0.0005	1755–1810	N	1752	13	26S, 14W	X1	1826	110	462	···	···
	17 Nov	<12	60	0.002	0950–0955	N	0947	10	17N, 21E	M7	dg	dg	dg	PS	1
	28 Dec	02	100	0.002	0040–0050	3	0039	9	20N, 56W	M5	0054	60	672	···	1
2000	9 Jan	14	60	0.006	1415–1420	N	···	···	N, 120W	···	dg	dg	dg	PS	4
	18 Jan	18	110	0.009	1710–1735	N	1707	20	19S, 11E	M4	1754	120	739	530	···
	12 Feb	05	80	0.009	0405–0420	3	0351	19	26N, 24W	M1	0431	110	1107	810	···
	17 Feb	21	120	0.009	2025–2040	3	2017	18	29S, 07E	M1	2130	360	728	570	···
	18 Feb	10	150	0.075	0925–0930	N	···	···	N, 120W	···	0954	80	890	PS	2
	2 Mar	09	120	0.006	0825–0835	2	0820	8	14S, 52W	X1	1154	60	776	···	1
	3 Mar	03	120	0.004	0215–0225	0	0208	6	15S, 60W	M4	0230	80	841	···	1

Table 1. (continued)

	Proton Event						Flare Event				CME				
	Time[a]		E[b]		Type III Time[d]	Type II	Start	Rise	H α	X-ray	First Obs.	Size[g]	Speed	Shock Speed[h]	
Year	Date(s)	Hour	(MeV)	Intensity[c]	(UT)	Int.[e]	(UT)	(min)	Position	Peak[f]	(UT)	(deg)	(km/s)	(km/s)	Group[i]
	22 Mar	20	80	0.004	1845–2015	N	1834	14	14N, 57W	X1	1931	80	478	···	···
	24 Mar	10	80	0.002	0750–0755	2	0741	11	15N, 82W	X2	dg	dg	dg	···	···
	4 Apr	16	80	0.117	1515–1535	N	1512	29	16N, 66W	C9	1632	60	1188	870	4
	23 Apr	14	150	0.007	~1225	N	···	···	N, 120W	···	1230	120	1187	PS	···
	27 Apr	16	60	0.0007	~1420	N	1404	36	N, 95W	C1	1430	50	1110	···	···
	1 May	11	50	0.0009	1020–1025	0	1016	11	20N, 54W	M1	1054	20	1360	···	1
	4 May	12	60	0.001	1100–1105	2	1057	11	20S, 90W	M8	1126	70	1404	···	1
	5 May	<20	50	0.001	1525–1530	N	···	···	N, 110W	M2	1550	120	1594	···	···
	10 May	<27	80	0.0006	1930–1945	N	1926	11	14N, 20E	C9	2006	130	641	603	···
	15 May	18	70	0.007	1600–1605	N	1546	15	22S, 68W	C8	1626	70	1212	···	1
	23 May	22	30	0.002	2045–2050	0	2048	5	23N, 41W	M1	2130	50	475	ps	1
	6 Jun	<18	150	0.02	1510–1545	N	1458	27	20N, 14E	X2	1554	180	1119	990	5
	10 Jun	18	200	0.79	1700–1715	N	1640	22	22N, 40W	M5	1708	120	1108	PS	2
	15 Jun	21	30	0.001	1945–1950	N	1938	19	20N, 62W	M2	1950	70	1081	···	1
	17 Jun	05	70	0.004	~0230	0	0225	12	22N, 72W	M4	0328	60	927	···	1
	18 Jun	26	70	0.014	0150–0155	N	0152	7	23N, 85W	X1	0210	70	629	···	1
	23 Jun	16	70	0.008	1420–1425	0	1418	13	23N, 72W	M3	1454	60	847	···	1
	25 Jun	12	70	0.007	0740–0745	1	0717	35	16N, 55W	M2	0754	70	1617	···	3
	28 Jun	20	70	0.0006	1845–1905	N	1848	22	N, 95W?	C4	1931	90	1198	···	1
	10 Jul	24	70	0.002	2125–2130	3	2105	37	18N, 49E	M6	2150	130	1352	PS	···
	14 Jul	11	900	45	1020–1050	2	1003	19	22N, 07W	X6	1054	360	1674	1600	4
	22 Jul	12	150	0.19	1130–1135	2	1117	17	14N, 56W	M4	1154	80	1230	···	3
	27 Jul	24	120	0.031	~1930	N	···	···	N, 120W	···	1954	360	905	PS	···
	9 Aug	<50	60	0.0001	1525–1545	N	1519	62	11N, 11W	C2	1630	360	702	805	5
	12 Aug	11	60	0.003	1000–1005	2	0945	11	17S, 79W	M1	1035	60	662	PS	1
	4 Sep	<20	···	1e–5	0545,0625	0	0649	3	12N, 37W	C1	0606	90	849	713	5
	7 Sep	21	60	0.001	~2055	2	2032	23	06N, 47W	C7	2130	90	422	···	···
	9 Sep	10	70	0.003	~0830	3	0828	21	07N, 67W	M2	0856	70	554	···	···
	12 Sep	13	150	0.64	1145–1150	1	1131	42	17S, 09W	M1	1154	100	1550	640	2
	19 Sep	11	70	0.004	0810–0820	1	0806	20	14N, 46W	M5	0850	60	766	···	1
	9 Oct	<30	70	0.002	2320–2345	2	2319	24	01N, 14W	C7	2350	360	798	590	5
	16 Oct	07	120	0.12	~0650	N	0640	48	N, 95W	M2	0727	90	1336	···	2
	25 Oct	13	120	0.065	~0955	N	0845	160	S, 120W	C4	0826	130	770	580	3
	29 Oct	<12	70	0.0003	0150–0210	2	0128	29	25S, 35E	M4	dg	dg	dg	650	5
	8 Nov	23	300	···	2255–2335	0	2242	46	10N, 75W	M7	2306	120	1738	1300	4
	24 Nov	06	300	0.07	0500–0525	3	0455	7	22N, 03W	X2	0530	360	1289	PS	3
	24 Nov	16	300	0.9	1455–1525	1	1451	22	22N, 07W	X2	1530	360	1245	PS	2
	25 Nov	<18	300	···	0100–0135	3	0059	32	07N, 50E	M8	0131	120	2519	1000	5
	28 Dec	15	120	0.007	~1205	N	···	···	N, 120W	···	1206	360	930	···	···
2001	5 Jan	19	70	0.01	~1650	N	···	···	N, 120W	C2	1706	140	828	···	···
	20 Jan	<29	120	0.003	1845–1855	3	1833	14	08S, 41E	M1	1932	130	1507	680	5
	26 Jan	14	50	0.001	1150–1155	2	1150	16	27S, 57W	C2	1206	40	928	···	···
	28 Jan	17	150	0.29	1540–1605	N	1540	20	04S, 59W	M2	1554	120	916	630	2
	11 Feb	03	70	0.0048	0100–0110	2	0057	26	24N, 57W	C7	0131	80	1183	PS	···
	26 Feb	08	60	0.0048	~0505	N	···	···	N, 120W	···	0754	100	851	···	1
	10 Mar	08	60	0.002	0400–0410	2	0400	5	27N, 42W	M7	0426	20	819	···	1
	25 Mar	<22	30	0.0001	1635–1700	N	1625	11	16N, 23E	C9	1706	360	677	850	5
	29 Mar	12	150	0.24	1000–1015	2	0957	18	16N, 12W	X2	1026	360	942	700	2
	2 Apr	13	150	0.03	1100–1105	3	1058	38	16N, 62W	X1	1126	50	992	PS	2
	2 Apr	23	400	3.9	2145–2215	3	2132	19	17N, 78W	X20	2206	100	2505	1020	2
	9 Apr	16	300	0.043	1525–1545	3	1520	14	21S, 04W	M8	1554	360	1192	PS	2
	10 Apr	07	300	1.07	0510–0540	3	0506	20	23S, 09W	X2	0530	360	2411	1290	4
	12 Apr	12	300	0.34	1015–1045	3	0939	49	20S, 42W	X2	1031	120	1184	PS	2
	14 Apr	18	···	···	1710–1800	N	1715	···	17S, 71W	M1	1754	50	830	···	1
	15 Apr	14	900	12.2	1345–1415	3	1319	31	20S, 84W	X14	1406	110	1199	700	2
	18 Apr	03	900	2.9	0220–0240	3	0212	64	S, 120W	C2	0230	140	2465	···	2
	26 Apr	<22	30	0.0003	1305–1310	0	1126	106	17N, 31W	M8	1230	360	1006	1040	5
	7 May	13	90	0.15	~0855	N	···	···	N, 120W	···	1006	180	1223	ps	2
	20 May	08	150	0.14	0605–0615	3	0600	3	17S, 91W	M6	0626	90	546	···	2
	29 May	<24	40	0.0001	2355–2415	N	···	···	S, E120	···	2406	90	2087	···	···
	4 Jun	17	70	0.016	1625–1635	2	1611	22	22N, 60W	C3	1630	80	464	ps	···
	11 Jun	<14	45	0.0006	0540–0545	2	0533	19	16S, 34W?	C7	0606	···	326	···	1
	15 Jun	11	60	0.001	1005–1020	2	1001	12	26S, 41E	M6	1032	50	1090	PS	1
	15 Jun	15	120	0.28	~1530	N	···	···	S, 120W	···	1556	130	1701	PS	3
	18 Jun	27	100	0.004	2220–2230	0	2150	71	10S, 23W	C5	0354	30	1301	···	···
	19 Jul	11	40	0.0003	~1000	0	0952	12	12S, 62W	M2	1030	40	1668	···	1
	9 Aug	16	70	0.013	···	N	N, W00?	1030	160	479	640	5			
	14 Aug	18	60	0.001	1145–1200	2	1130	72	110W	C2	1601	360	618	···	···

Table 1. (continued)

	Proton Event						Flare Event				CME				
	Time[a]		E[b]		Type III Time[d]	Type II	Start	Rise	H α	X-ray	First Obs.	Size[g]	Speed	Shock Speed[h]	
Year	Date(s)	Hour	(MeV)	Intensity[c]	(UT)	Int.[e]	(UT)	(min)	Position	Peak[f]	(UT)	(deg)	(km/s)	(km/s)	Group[i]
	15 Aug	25	500	5.7	~2355	N	···	···	S, 120W	···	2354	180	1575	PS	4
	12 Sep	23	30	0.0005	2135	N	···	···	16S, 62W?	M1	2206	30	668	PS	1
	15 Sep	12	120	0.073	1135–1200	2	1104	24	27S, 53W	M2	1154	80	478	···	···
	17 Sep	<12	60	0.0009	0820–0830	3	0818	7	14S, 04E	M2	0854	50	1009	···	···
	24 Sep	11	400	8.49	1020–1040	0	0932	66	16S, 23E	X3	1030	120	2402	1220	4
	1 Oct	<12	120	1.89	0440–0520	0	0441	24	S, 95W	M9	0530	80	1405	PS	4
	5 Oct	<17	60	0.03	1025–1030	0	···	···	S, 110W	C2	1030	120	1537	···	···
	9 Oct	08	60	0.02	0735–0755	2	···	···	S, 120W	···	0806	70	526	PS	1
	9 Oct	<14	70	0.012	1050–1130	2	1046	27	25S, 10E	M1	1130	120	973	780	···
	19 Oct	01	150	0.04	0100–0130	3	0047	18	16N, 18W	X2	0127	180	558	PS	···
	19 Oct	16	150	0.076	1630–1700	2	1613	17	15N, 29W	X2	1650	160	901	870	4
	22 Oct	04	60	0.0003	0030–0040	0	0022	18	17N, 57W	M1	0050	20	772	PS	1
	22 Oct	15	150	0.16	1500–1530	2	1427	41	21S, 18E	M7	1506	140	1336	640	2
	4 Nov	17	900	16.8	1615–1640	2	1603	17	06N, 18W	X1	1635	360	1810	1250	4
	17 Nov	07	50	0.01	0500–0530	1	0449	36	13S, 42E	M3	0530	160	1379	680	5
	22 Nov	21	100	0.21	2025–2045	3	2018	18	25S, 67W	M4	2058	120	1443	PS	···
	22 Nov	25	900	2.7	2305–2330	0	2232	58	15S, 34W	X1	2330	270	1437	1320	4
	28 Nov	<20	50	0.002	1630–1650	1	1626	9	04N, 16E	M7	1730	90	500	ps	···
	11 Dec	<14	50	0.001	~0830	N	···	···	S, 120W	···	0954	100	891	···	···
	25 Dec	<22	40	0.0005	~1100	1	···	···	S, 120E	···	1130	120	1773	···	···
	26 Dec	06	500	6.3	0510–0600	3	0432	68	08N, 54W	M7	0530	90	1446	580	2
	28 Dec	<24	50	0.21	2000–2040	2	2002	43	S, 100E	X3	2006	120	2216	870	···
2002	8 Jan	<24	70	0.004	1805–1840	N	1814	131	N, 120E	M1	1754	90	1794	900	5
	14 Jan	<08	70	0.05	~0535	1	0529	58	S, 100W	M4	0540	130	1492	···	3
	27 Jan	12	90	0.083	~1200	N	···	···	N, 120W	···	1230	70	1136	···	2
	20 Feb	06	80	0.09	0555–0630	1	0552	20	12N, 72W	M5	0630	50	952	···	1
	10 Mar	<28	40	0.0003	2240–2300	0	···	···	S, 100E	M2	2304	130	1429	···	···
	15 Mar	24	70	0.005	2240–0255	0	2209	61	08S, 03W	M2	2306	360	911	670	5
	18 Mar	04	80	0.028	0215–0220	1	0216	15	S, 100W?	M1	0254	160	989	710	2
	22 Mar	12	60	0.003	1030–1115	2	1012	62	S, 90W	M2	1106	130	1750	660	4
	11 Apr	16	70	0.005	1615–1630	2	1616	10	15S, 33W	C9	1650	50	540	···	···
	14 Apr	12	50	0.002	0725–0735	3	0728	11	19N, 57W	M1	0750	50	757	···	1
	15 Apr	03	30	···	0250–0255	N	0246	5	15S, 79W	M1	0306	45	674	···	1
	17 Apr	08	80	0.09	0750–0900	2	0746	38	14S, 34W	M3	0826	70	1240	860	4
	21 Apr	00	500	5.4	0112–0215	2	0043	68	14S, 84W	X2	0127	120	2393	800	4
	30 Apr	<25	40	0.003	~2220	N	···	···	S, 120W	···	2326	170	1103	···	···
	20 May	15	50	0.002	1525–1535	3	1521	6	21S, 65E	X2	1550	30	553	ps	···
	22 May	06	60	0.03	0325–0400	0	0318	36	22S, 53W	C5	0350	120	1557	1320	5
	30 May	03	40	0.0005	~0500	N	0424	68	N, 100W	M1	0506	50	1625	···	1
	4 Jul	20	39	0.001	~1940	0	···	···	S, 120W	···	2006	120	957	···	···
	7 Jul	12	···	0.2	~1120	N	1115	28	S, 95W	M1	1106	85	1423	···	3
	9 Jul	19	50	0.004	~1830	N	···	···	S, 120W	···	1931	110	1076	···	1
	15 Jul	<30	120	0.0001	2000–2005	0	1959	9	14N, 01E	X3	2045	100	1151	960	5
	20 Jul	<34	90	0.022	2105–2135	3	2104	26	S, 100E	X3	2206	120	1941	1300	5
	3 Aug	19	40	0.0007	1900–1915	0	1859	8	16S, 76W	X1	1932	30	1150	···	1
	5 Aug	07	45	0.001	0640–0645	0	···	···	07S, 45W?	C2	0732	20	689	···	1
	14 Aug	03	70	0.009	0145–0205	3	0147	25	09N, 54W	M2	0230	60	1309	···	1
	16 Aug	07	70	0.004	~0600	2	0546	25	06N, 83W	M3	0606	70	1378	PS	1
	16 Aug	<15	70	0.009	1200–1230	2	1132	60	14S, 20E	M5	1230	160	1585	770	5
	18 Aug	20	90	0.02	2115–2130	2	2112	13	12S, 19W	M2	2154	100	682	ps	1
	19 Aug	10	60	0.017	1030–1035	0	1028	6	12S, 25W	M3	1106	80	549	ps	1
	20 Aug	08	150	0.04	0825–0830	0	0822	8	10S, 38W	M3	0854	40	1099	ps	1
	22 Aug	02	120	0.3	0150–0205	2	0147	10	07S, 62W	M5	0206	80	998	···	2
	24 Aug	00	900	1.7	0055–0115	2	0049	23	02S, 81W	X3	0127	150	1913	710	2
	5 Sep	<20	120	0.01	1620–1635	2	1618	28	09N, 28E	C5	1654	160	1748	880	5
	24 Sep	11	50	0.0009	1130–1135	0	···	···	S, 120W	···	1130	20	1104	···	1
	27 Sep	02	50	0.001	0125–0130	N	0118	30	S, 95W	C5	0154	40	1502	···	1
	20 Oct	14	30	0.0004	1410–1415	2	1410	3	13S, 63W	C7	1430	10	1011	···	1
	9 Nov	15	70	0.2	1305–1405	2	1308	15	12S, 29W	M5	1331	90	1838	900	4
	24 Nov	<20	40	3e–5	2005–2010	1	2014	15	17N, 34E	C6	2030	120	1077	PS	5
	19 Dec	22	120	0.04	2140–2200	3	2134	19	15N, 09W	M3	2206	120	1092	···	1
	22 Dec	<03	30	0.0009	0255–0300	2	0214	38	23N, 42W	M1	0330	80	1071	850	···
2003	17 Mar	19	40	0.003	1900–1905	0	1850	15	14S, 39W	X2	1954	50	1020	PS	1
	18 Mar	14	60	0.004	1215–1220	2	1157	17	09S, 46W	X2	1354	80	1601	PS	1
	7 Apr	<08	40	0.001	~0930	0	0925	65	10S, 88W	B7	0950	40	217	···	1
	21 Apr	17	70	0.002	1300–1315	3	1302	13	16N, 02E	M3	1336	120	784	···	1
	23 Apr	00	75	0.007	0100–0115	2	0045	17	22N, 25W	M5	0127	70	916	···	···

Table 1. (continued)

	Proton Event						Flare Event				CME				
	Time[a]		E[b]		Type III Time[d]	Type II	Start	Rise	H α	X-ray	First Obs.	Size[g]	Speed	Shock Speed[h]	
Year	Date(s)	Hour	(MeV)	Intensity[c]	(UT)	Int.[e]	(UT)	(min)	Position	Peak[f]	(UT)	(deg)	(km/s)	(km/s)	Group[i]
	24 Apr	12	65	0.008	~1300	2	1245	8	21N, 39W	M3	1327	45	609	···	···
	25 Apr	<18	50	0.0005	0525–0540	2	0523	17	16N, 66E	M1	0550	90	806	···	···
	27 May	22	70	0.0003	2255–2310	3	2256	11	07S, 17W	X1	2350	360	964	PS	1
	28 May	00	120	0.04	0020–0035	0	0017	10	06S, 20W	X4	0127	220	1366	1000	1
	31 May	03	120	0.2	0225–0230	3	0213	11	07S, 65W	M9	0230	150	1835	···	1
	15 Jun	<24	30	0.0001	2345–2400	2	2325	31	07S, 80E	X1	2354	130	2053	730	5
	10 Jul	14	30	0.0003	1355–1400	3	1354	18	13N, 91W	M4	<1633	dg	877	···	1
	17 Jul	11	30	0.0002	0820–0840	2	···	···	15N, 20E	M1	0854	360	531	···	1
	19 Aug	03	50	0.001	0755–0800	2	0738	21	12S, 64W	M2	0830	40	412	···	1
	21 Oct	<09	40	0.0008	0350–0400	3	···	···	S, 100E	···	0354	120	1484	PS	5
	26 Oct	07	70	0.0006	0645–0700	3	0557	57	15S, 44E	X1	0654	70	1371	PS	···
	26 Oct	18	150	3.5	1735–1805	2	1703	58	02N, 38W	X1	1754	130	1537	1330	4
	28 Oct	12	900	40	1105–1120	2	0951	79	16S, 08E	X17	1054	360	2459	2200	4
	29 Oct	22	900	31	2035–2050	3	2037	12	15S, 02W	X10	2054	360	2029	2100	4
	2 Nov	10	90	0.2	0920–0930	1	···	···	S, 120W	···	0930	120	2036	PS	4
	2 Nov	18	900	20	1715–1735	2	1703	22	14S, 56W	X8	1730	130	2598	1130	4
	4 Nov	21	100	0.7	1935–2000	3	1929	21	19S, 83W	X28	1954	130	2657	880	4
	7 Nov	16	···	0.04	dg 1500?	N	1500	140	S, 110W	B5	1554	dg	2237	···	···
	18 Nov	11	50	0.004	0725–0745	3	0723	29	00S, 18E	M3	0806	80	1223	PS	1
	20 Nov	07	90	0.02	0735–0745	0	0735	12	03N, 08W	X1	0806	90	669	PS	1
	2 Dec	12	70	0.1	~1015	N	1000	···	S, 95W	C8	1026	100	1393	···	3
	31 Dec	18	60	0.0008	1825–1830	N	···	···	···99W	M1	dg	dg	dg	···	1
2004	7 Jan	<14	50	0.0003	1015–1025	2	1014	13	02N, 69E	M8	1030	70	1822	···	···
	4 Feb	11	60	0.002	1115–1120	3	1112	6	07S, 49W	M1	1154	20	764	···	1
	11 Apr	05	120	0.11	0400–0425	0	0354	25	16S, 46W	M1	0430	90	1645	1100	2
	4 Jun	<10	50	0.0006	0730–0735	2	···	···	N, 120W	···	0750	100	1306	···	1
	13 Jul	01	70	0.008	0015–0035	2	0009	8	14N, 59W	M7	0054	60	409	···	···
	22 Jul	<12	120	0.008	0740–0745	0	0741	18	4N, 10E	C5	0830	50	899	PS	1
	25 Jul	16	120	0.2	1440–1505	1	1419	55	4N, 33W	M2	1454	130	1333	1300	5
	29 Jul	<23	60	0.005	~1225	0	1142	82	14S, 83W	C2	1206	60	1180	PS	5
	31 Jul	<27	60	0.02	~0615	0	0516	101	S, 95W	C8	0554	100	1192	PS	···
	30 Aug	03	30	4e–5	0305–0310	3	0304	7	7N, 72W	C2	0354	40	362	···	1
	2 Sep	26	55	0.0007	2355–0005	N	···	···	S, 120W	···	0030	360	751	···	···
	12 Sep	<04	50	0.005	0025–0100	2	0004	52	4N, 42E	M5	0036	140	1328	960	5
	19 Sep	18	60	0.4	1650–1720	2	1646	26	3N, 58W	M2	dg	dg	dg	690	4
	30 Oct	07	60	0.008	0610–0615	3	0608	10	14N, 42W	M4	0654	90	422	···	1
	30 Oct	13	60	0.002	1140–1145	0	1138	8	12N, 26W	X1	1230	90	427	···	1
	30 Oct	17	60	0.01	1625–1630	N	1618	15	13N, 28W	M6	1654	90	690	···	1
	1 Nov	07	120	1.3	~0600	0	···	···	S, 120W	···	0606	115	925	···	2
	4 Nov	<29	90	0.0002	2255–2305	0	2253	16	11N, 19E	M5	2330	140	1055	720	5
	7 Nov	17	200	1	1600–1650	1	1542	24	9N, 17W	X2	1654	150	1759	830	4
	9 Nov	19	200	0.2	1700–1720	1	1659	20	7N, 51W	M9	1726	130	2000	PS	4
	10 Nov	03	500	1.1	0210–0220	3	0159	14	9N, 49W	X3	0226	120	2000	1080	4
	2 Dec	<27	70	0.028	2350–0005	3	2349	22	9N, 03E	M2	0026	360	1216	760	5
2005	14 Jan	11	50	0.0002	1005–1020	0	1008	20	06S, 04E	C9	1130	20	396	···	1
	15 Jan	06	120	0.07	0605–0630	2	0554	44	11N, 06E	M9	0630	90	2049	···	3
	15 Jan	23	120	0.6	2230–2305	3	2224	42	15N, 05W	X3	0654	130	2861	1200	4
	17 Jan	10	200	36	0905–0955	3	0659	173	15N, 25W	X4	0930	110	2094	1170	4
	20 Jan	06	900	30	0645–0705	3	0636	25	14N, 61W	X7	0654	80	~2500	1210	2
	6 May	03	40	0.003	0305–0315	0	0305	9	04S, 71W	C9	0330	20	1120	PS	1
	6 May	12	40	0.003	1115–1130	0	1111	17	04S, 76W	M1	1154	30	1144	PS	1
	11 May	20	60	0.005	1925–1930	2	1922	16	10S, 55W	M1	2013	70	550	···	···
	13 May	17	80	0.02	1640–1700	2	1613	44	12N, 11E	M8	1722	360	1689	1270	5
	31 May	16	50	0.0005	1435–1440	2	1433	9	12N, 22W	C2	1532	30	313	···	···
	3 Jun	<29	40	5e–5	~1200	2	1151	35	15N, 90E	M1	1232	80	1679	···	···
	14 Jun	06	30	0.0007	0505–0520	0	0654	36	10N, 48W	C4	0724	100	791	PS	···
	16 Jun	20	500	0.5	2010–2020	2	2001	21	9N, 85W	M4	dg	dg	dg	···	2
	9 Jul	24	80	0.02	2200–2225	0	2147	19	11N, 27W	M3	2230	65	1540	PS	3
	12 Jul	19	50	0.0008	1639–1655	0	1547	37	11N, 67W	M2	1654	80	523	···	1
	13 Jul	05	40	0.0003	0235–0240	0	0235	41	18N, 82W	M1	0306	40	759	PS	1
	13 Jul	14	50	0.005	1400–1420	0	1401	48	11N, 78W	M5	1430	70	1423	PS	1
	14 Jul	11	70	0.6	~1030	0	1016	39	08N, 89W	X1	1030	80	2115	PS	4
	17 Jul	12	90	0.07	1120–1135	0	···	···	N, 120W	···	1130	120	1527	···	3
	21 Jul	08	50	0.002	~0330	0	···	···	N, 120W	···	0354	180	925	···	···
	24 Jul	<25	40	0.0004	1350–1420	2	···	···	N, 120E	···	1354	130	2528	530	5
	22 Aug	01	80	0.05	0100–0130	3	0044	49	09S, 48W	M3	0131	160	1194	790	2
	22 Aug	18	80	1.5	1655–1730	0	1646	51	12N, 60W	M6	1730	100	2378	PS	4

Table 1. (continued)

	Proton Event						Flare Event				CME				
	Time[a]		E[b]		Type III Time[d]	Type II	Start	Rise	H α	X-ray	First Obs.	Size[g]	Speed	Shock Speed[h]	
Year	Date(s)	Hour	(MeV)	Intensity[c]	(UT)	Int.[e]	(UT)	(min)	Position	Peak[f]	(UT)	(deg)	(km/s)	(km/s)	Group[i]
	29 Aug	12	70	0.02	~1100	N	···	···	S, 120W	···	1054	120	1600	···	3
	31 Aug	25	80	0.01	2200–2300	N	···	···	S, 120W	···	2230	360	1808	PS	3
	5 Sep	<13	30	0.001	0930–0935	0	0853	107	07S, 99E	C3	0948	100	2326	···	···
	7 Sep	<20	200	0.2	1735–1800	0	1717	23	06S, 89E	X17	dg	dg	dg	950	5
	13 Sep	22	7	0.63	1950–2000	0	1919	8	09S, 10E	X2	2000	130	1866	1220	4
2006	6 Jul	09	120	0.02	0815–0820	2	0813	23	11S, 32W	M3	0854	160	911	480	4
	6 Nov	15	60	0.001	1740–1745	2	1743	3	0N, 89E	C9	1754	70	1994	···	···
	21 Nov	20	30	0.0004	1925–1930	N	···	···	S, 120W	···	dg	dg	dg	···	1
	5 Dec	<15	70	0.03	1030–1100	N	1018	17	07S, 68E	M9	dg	dg	dg	PS	5
	6 Dec	<22	500	0.9	1840–1905	0	1829	18	06S, 64E	M7	dg	dg	dg	PS	5
	13 Dec	02	900	5.1	0225–0245	3	0214	26	06S, 23W	X3	0254	180	1774	1180	2
	14 Dec	22	300	0.5	2210–2225	3	2107	68	07S, 46W	X2	2230	70	1042	980	···

[a]Onset time of proton event. If the time is >23 h then the time is the following day. Times preceded by < indicate the the event had a slow rise.

[b]Maximum energy to which protons were detectable. These values are approximate and in some cases are based on data from the GOES HEPAD instrument. Events detected by neutron monitors are indicated by 900 MeV, although the actual maximum energy may have been considerably greater.

[c]Peak proton intensity within the first ~12 h in the ~25–30 MeV energy range in units protons/(cm^2 s sr MeV). Indeterminate values are indicated by an ellipsis.

[d]Start and end times of type III burst (at 14 MHz) to the nearest 5 min. Single times preceded by a tilde are ones in which there is no emission at 14 MHz and the time is the start time at lower frequencies. In the two events indicated by an ellipsis in this column, there was no radio emission at the time of solar event.

[e]Intensity of metric type II as given in SGD except for those cases in which there is no clear evidence in the dynamic spectra of a type II burst. In this case the intensity is given as 0. "N" indicates that original data were not available for examination.

[f]1–8 Å soft X-ray peak intensity in terms of B, C, M, and X nomenclature where these represent intensities of 10^{-7}, 10^{-6}, 10^{-5}, and 10^{-4} W m^{-2}, respectively. An ellipsis indicates that no event was observed.

[g]Angular size in the sky plane of the CME when it was about halfway through the LASCO C2 field of view.

[h]Average speed of the associated shock from the Sun to near Earth. PS in this column indicates there was a passing shock that was not related to the solar activity and for which there appears to be a related increase of particle intensity; ps indicates that there was a passing shock during the event but with no associated particle increase.

[i]Grouping of the event based on relative abundances, intensity, and profile. Group 1 events were electron-rich (proton-poor). Group 2 events were proton-rich and Fe-rich. Group 3 events were proton-rich, Fe-poor, and had no local shock enhancement. Group 4 events were proton-rich, Fe-poor, and had a local shock enhancement. Group 5 events had a slow rise peaking at shock passage. Events with few ions or preceded by another event producing a high background are indicated by ellipses.

2000 km/s, consistent with the speed determined by the CACTUS software (http://sidc.oma.be/cactus/). This lower speed was used.] The direction of CME propagation was used to determine the latitudes of the behind-the-limb events (north or south).

[15] The CME angular widths in the table are our own assessments made using the images linked to the CUA catalog. A main reason for reassessing the CME widths is that many of the SEP events are associated with what are reported as "halo" CMEs in the catalog, with angular widths of 360°. However, examination of the images indicates that the CMEs were not directed at Earth and were not true halo CMEs. We estimated angular sizes of the CMEs when their leading edges were about halfway through the C2 field of view.

[16] Table 1 also provides the transit speeds of the CME-driven shocks from the Sun to near Earth. Sometimes other shocks, not related to the SEP event, are seen in situ that may or may not produce an effect on the particles. Such passing shocks are indicated in the shock speed column as PS (passing shock with local shock-associated particle increase) or ps (passing shock with no particle increase).

3. Event Classification

[17] After careful examination of the data we divided the events into five groups based on the ratios *e*/*p* and Fe/O at event onset and the time profiles as described below. Seventy-nine of the 280 events could not be allocated to a group because of data gaps (11 events), a preceding high background or complex profile (21 events), or low intensities of >10 MeV/nucleon O and Fe ions (45 events). The group number is given in Table 1. As discussed further below, we emphasize that we are not dividing the events into five distinct groups but rather the groups help to illustrate the diversity of event properties.

3.1. Group 1

[18] The first group (80 events) we refer to as "electron-rich." The distribution of *e*/*p* ratios (Figure 1) defined as the ratio of the early peak intensities of ~0.5 MeV electrons to ~25 MeV protons (*e*/*p*) shows a continuum of values, with no distinct groups of relatively electron-rich and electron-poor events. We have chosen to use a criterion of $e/p \geq 8 \times 10^4$ (indicated by the dashed vertical line), which would just exclude the large ground level event on 6 May 1998 from group 1.

[19] Figure 2 shows data for a typical group 1 event on 28 December 1999. The top panel of the bottom section shows the soft X-ray intensity profile from the GOES spacecraft. The second panel shows electron data (gray curves) in two energy ranges (0.3–0.7 and 0.7–1 MeV) and ERNE proton and helium data (purple and green curves, respectively) at two energies (26–32 and 51–67 MeV/nucleon). The third panel

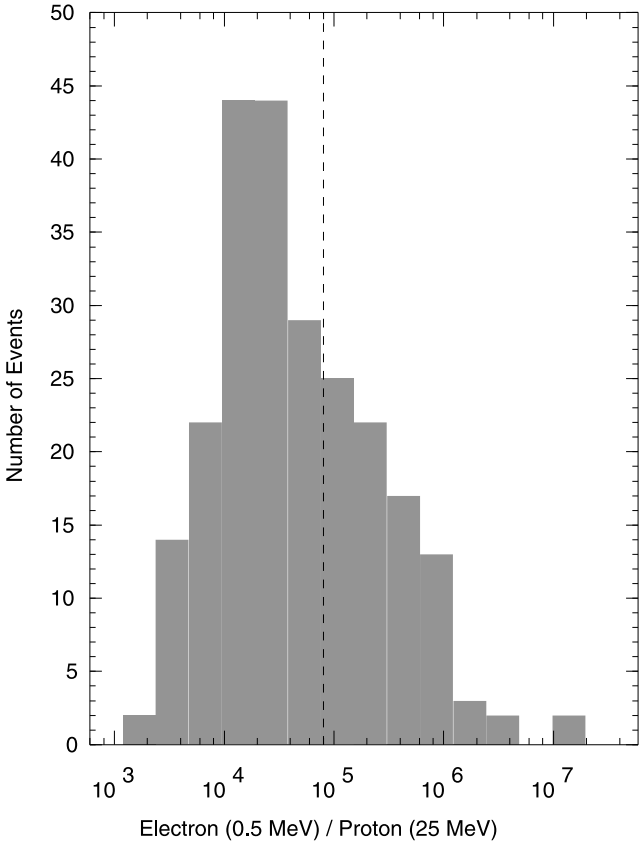

Figure 1. Histogram of the ratios of electron (~0.5 MeV) to proton (~25 MeV) intensities during the early stages of proton events extending above ~25 MeV in the period 1997–2006. Events to the right of the vertical dashed line are considered to be electron-rich and are assigned to group 1.

shows Fe (four shades from pink to red) and O (four shades of blue) at four energies [0.3–0.6, 1–3 MeV/nucleon (from ULEIS), and 14 and 34 MeV/nucleon (from SIS)]. The high-energy Fe and O intensities were calculated at these specific energies by a linear interpolation (in log-log space) of intensities in neighboring SIS energy ranges.

[20] It can seen that the event was associated with a very short duration flare (the vertical line shows the time of the flare) that was located at 6°N, 56°W, and was listed in SGD as lasting for 11 min in H α. Given the location and the rapid rise in the particle intensities, it can be reasonably assumed that Earth was magnetically connected to the flaring region. For the event in Figure 2, the three pairs of O and Fe curves at the bottom fall almost on top of each other, indicating Fe/O ratios of about 1. However, not all group 1 events were also Fe-rich. Of the 44 events with an Fe/O value determined at ~0.8 MeV/nucleon, 8 events had Fe/O < 0.25. Thus, although most of the group 1 events are both electron- and Fe-rich and so would belong to the "impulsive" class in the simple two-class paradigm, not all events in group 1 would be so classified. We note the event in Figure 2 does not appear in *Reames and Ng*'s [2004] list of "large impulsive SEP events" in the 2–10 MeV/nucleon range, most likely because it follows very closely a number of smaller events and is not clearly resolved at these lower energies, as may be seen in the bottom panel of Figure 2. However, it is very clear at energies above 10 MeV/nucleon.

[21] Like all 280 events in Table 1, the impulsive event of Figure 2 was associated with a CME. This CME had a speed of 672 km/s and an angular size of 45°. The meter wavelength radio emission was composed of a strong type III

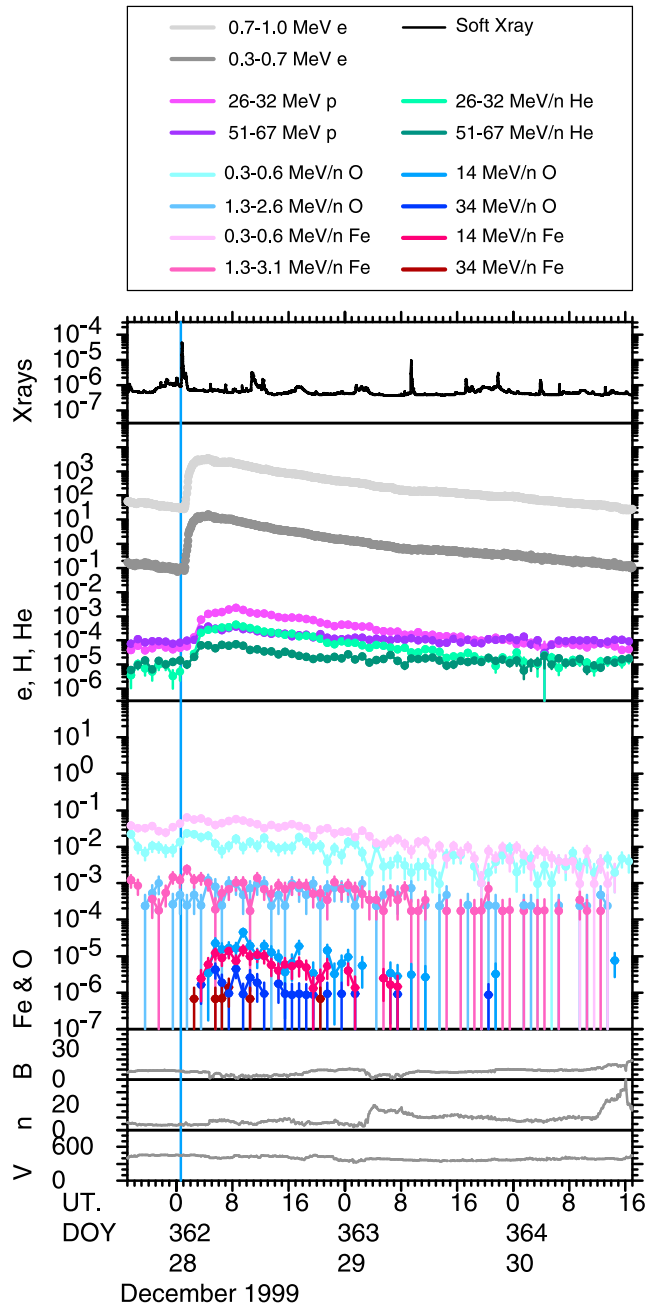

Figure 2. Intensity-time profiles for a range of particle species and energies (shown in legend) for an event in group 1. The top panel of the bottom part shows the 1–8 Å soft X-ray intensity profile (in W/m^2). The time of the flare of interest is indicated by a blue vertical line. The bottom three panels show the solar wind field magnitude B (in nT), density n (in cm^{-3}), and speed V (in km/s).

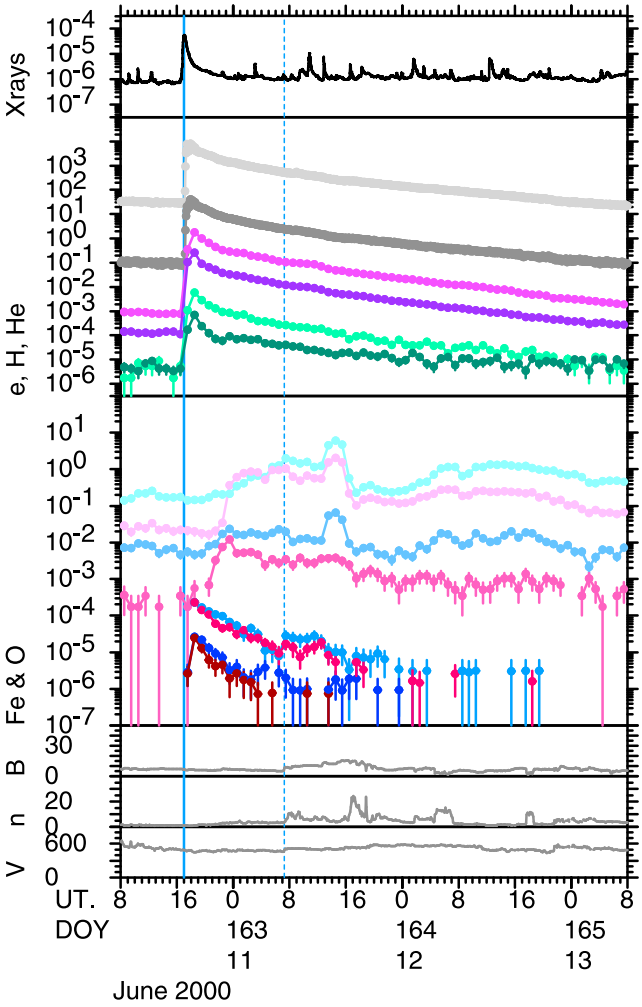

Figure 3. Intensity-time profiles for an event in group 2 in the same format as Figure 2. Note how much more intense the protons are relative to the electrons (purple and gray curves, respectively, in middle panel) in comparison with the event in Figure 2. The dashed blue vertical line indicates the time of passage of a weak shock seen as a small jump in *B*, *n*, and *V*.

emission at the start of the flare followed by type II emission. The radio data are presented in Figure 2b in the work of *Cane et al.* [2002] and show that the type III emission continued strongly to kilometer wavelengths. However, there were no type II emissions extending into the WAVES data.

[22] The bottom three panels of Figure 2 show solar wind data (magnetic field magnitude, and solar wind density and speed). During the period illustrated, the solar wind was relatively undisturbed and no shocks were observed.

[23] We note that two group 1 events (on 28 and 31 May 2003) would be considered "gradual" events because they are associated with relatively strong interplanetary shocks and the lower energy particles peak at shock passage. However, at the start of the event they were definitely electron–rich.

3.2. Group 2

[24] Events were allocated to group 2 if they were not in group 1 but were "Fe–rich." By Fe–rich we mean that the ratio of the peak of the early Fe intensity to the peak of the early O intensity was >0.24 at 34 MeV/nucleon or at 14 MeV/nucleon for some of the weaker events. Recall that the nominal Fe/O ratios for gradual events [*Reames*, 1988] and for the solar wind [*von Steiger et al.*, 2000] are both ~0.1, so Fe-rich in this work means that Fe/O is enhanced by more than a factor of 2. There were 37 events in group 2 and an example is shown in Figure 3. For this event on 10 June 2000, we determined a peak Fe/O ratio at 34 MeV/nucleon of 0.8. (For comparison, the event-averaged Fe/O above 25 MeV/nucleon was determined by *Cane et al.* [2006] to be 0.79.) This event was associated with an M5 flare at 1640 UT and 22°N, 40°W. The associated CME had a speed of 1108 km/s and an angular size of 120°. Type II emission was reported (in SGD) at meter wavelengths but the original records are not available to verify the exact nature of the emissions. There was no interplanetary type II emission, as indicated by the absence of emission at

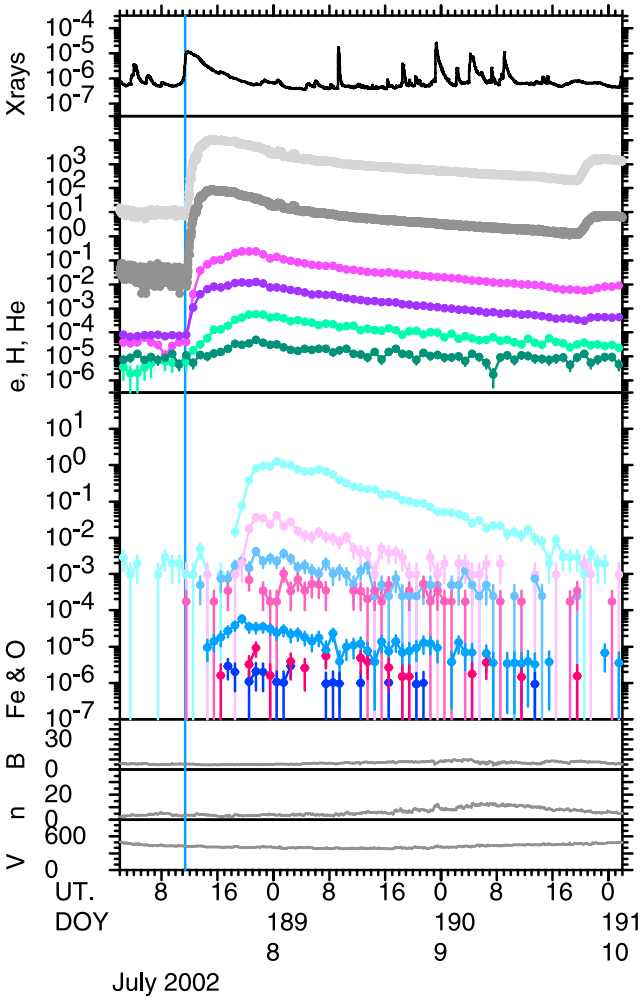

Figure 4. Intensity-time profiles for an event in group 3 in the same format as Figure 1. In contrast with the previous two events, there is no energy at which the Fe and O intensities are similar, indicating that Fe/O <1. No shocks passed the spacecraft during this interval and the solar wind was very quiet.

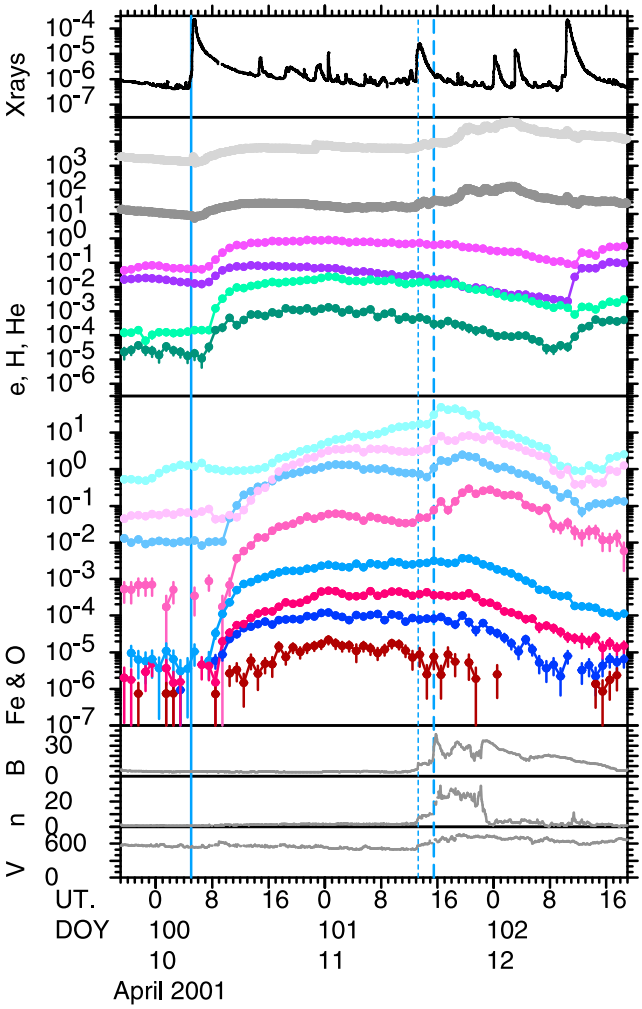

Figure 5. Intensity-time profiles for an event in group 4. Two shocks were seen during the event; the second vertical dashed line, with the longer dashes, indicates the associated shock, whereas the dotted line indicates the time of a passing shock.

kilometer wavelengths,and there was no associated shock at Earth. Either the CME direction of propagation was such that its shock and associated radio emissions were not detectable near Earth or, less likely, the CME did not drive a shock in the interplanetary medium. There was a passing unassociated shock on 11 June near Earth (dashed vertical blue line) that produced a small increase in the lowest-energy Fe and O intensities. The shock is clearly not associated with the 10 June event because a very fast transit speed of 3100 km/s would be implied, which is inconsistent with the modest particle increase and the in situ solar wind speed of ~500 km/s.

[25] It is interesting to compare the events in Figures 2 and 3. Although the electron and helium intensities (gray and green curves) are quite similar, the proton intensities (purple curves) are much lower in Figure 2. Hence, it may be more correct to describe the event in Figure 2 as being proton-poor rather than electron-rich.

3.3. Groups 3 and 4

[26] Events in groups 3 and 4 were neither electron-rich nor Fe-rich. For events in group 3, either no possibly associated shocks arrived at 1 AU (15 events) or in two cases the shocks were weak and produced little effect on the particle intensities. In some of the remaining cases, a passing shock was observed that was associated with another listed event. For example, the event on 9 November 2004 included a passing shock most likely associated with the event on 10 November. No shock likely to be associated with the 9 November event was observed, perhaps because this shock was overtaken by and merged with the shock from the 10 November event. For the majority of group 4 events (25 out of 31), a shock that probably originated in the same solar event was observed in situ and a significant particle enhancement was observed at shock passage. For the remaining six events there was also a shock-associated enhancement but the shock was "passing" and did not originate in the

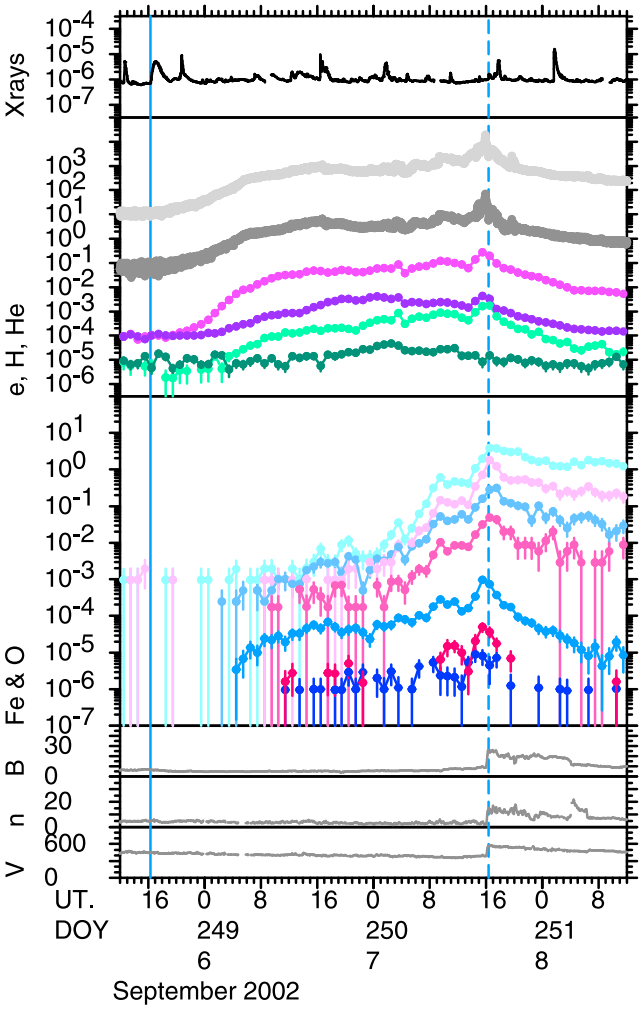

Figure 6. Intensity-time profiles for an event in group 5 in the same format as Figure 2. The ions reach peak intensities at the time the associated shock passes the spacecraft. The peaks at this time in electrons are caused by proton contamination.

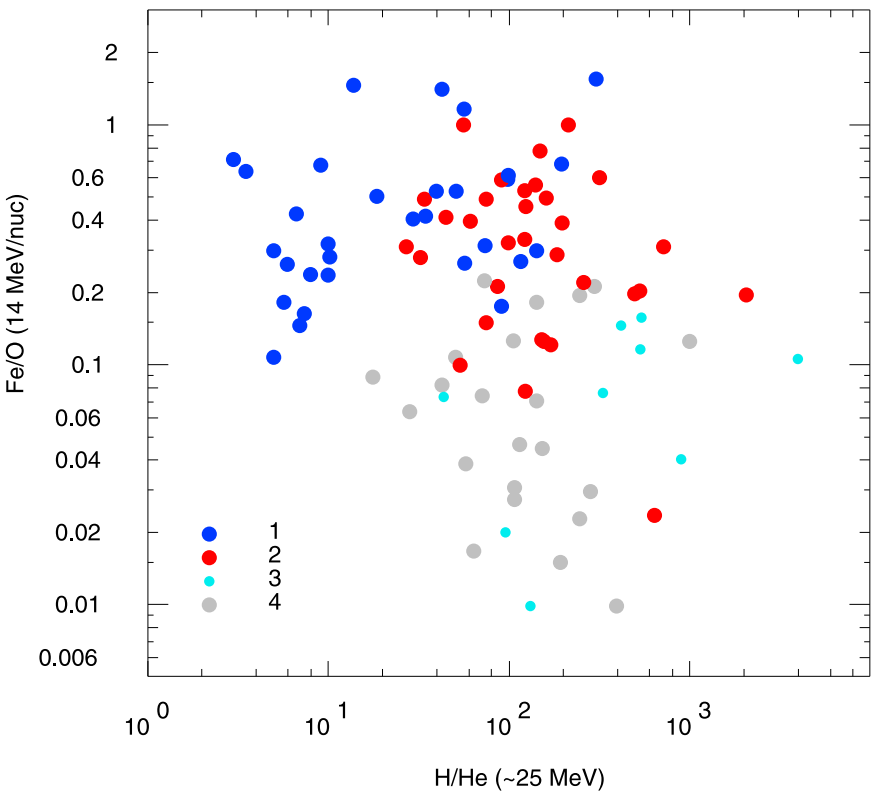

Figure 7. Early Fe/O ratios (at 14 MeV/nucleon) as a function of early H/He ratios (~25 MeV/nucleon) with color indicating the group to which the event belongs. Only the group 1 (dark blue) events are electron-rich. Note the considerable scatter and the absence of two distinct abundance combinations (Fe/O ~ 1 together with H/He ~ 10 or Fe/O ~ 0.1 together with H/He ~ 100).

same solar event as the prompt particles. Figure 4 shows an example of a group 3 event that occurred on 7 July 2002. No H α flare or metric radio emissions were observed, indicating that this was a behind-the-limb event although the relatively intense (M1) X-ray flare suggests the event originated not too far behind the limb. The associated CME observed above the southwest limb had a speed of 1423 km/s but the radio emissions at kilometer wavelengths were rather minor, lasting for an hour or so.

[27] The group 4 event of 10 April 2001 (Figure 5) had an early Fe/O ratio at 34 MeV/nucleon of 0.2 (and an event-averaged Fe/O above 25 MeV/nucleon of 0.126 [*Cane et al.*, 2006]). The X-ray flare was more intense and longer lasting than for the previously illustrated events and the CME was faster (2411 km/s). The 10 April 2001 event originated near 23°S, 9°W and the CME, which surrounded the coronagraph occulting disk, was directed at Earth. A strong shock reached Earth at the time indicated by the second vertical dashed line in Figure 5. This shock generated radio emission at kilometer wavelengths that lasted for about 20 h. The dotted line indicates another unrelated shock. At meter wavelengths the radio emission was composed of many type III bursts lasting some 20 min.

3.4. Group 5

[28] Group 5 events are characterized by slowly rising profiles peaking at the passage of a shock at 1 AU. The event illustrated in Figure 6 was associated with a C5 flare at 9°N, 28°E that occurred on 5 September 2002. The CME had a speed of 1748 km/s and the associated shock arrived at 1 AU on 7 September (dashed line). Of the ions illustrated, only the 50 MeV/nucleon He (dark green) did not peak at shock passage. The shock-generated radio emission was still in evidence when the shock reached 1 AU. At meter wavelengths the main activity was type III.

4. Statistical Results

4.1. Abundance Ratios

[29] Figure 7 shows Fe/O (at 14 MeV/nucleon) versus H/He (at ~25 MeV/nucleon) with the colors referring to events in the different groups. The ratios are for the early intensities as described earlier and for many events this is also the peak overall intensity. Only groups 1, 2, 3, and 4 are shown (colors blue, red, pale blue, and gray, respectively) because, by definition, the slow-rising group 5 events do not have significant early particles. It can be seen that there are clear tendencies for events in the different groups to appear in different parts of the scatterplot. Nevertheless, whereas the majority of the group 1 (dark blue) events (i.e., electron–rich events) are also Fe–rich, with Fe/O >0.24, H/He for these events spreads over two orders of magnitude from 3 to 300. Furthermore, whereas the other events do have H/He clustering around the canonical 'gradual' value of 100 [e.g., *Reames*, 1995] there is also a large range. Note that the group 2 events, which are Fe–rich by definition, are not

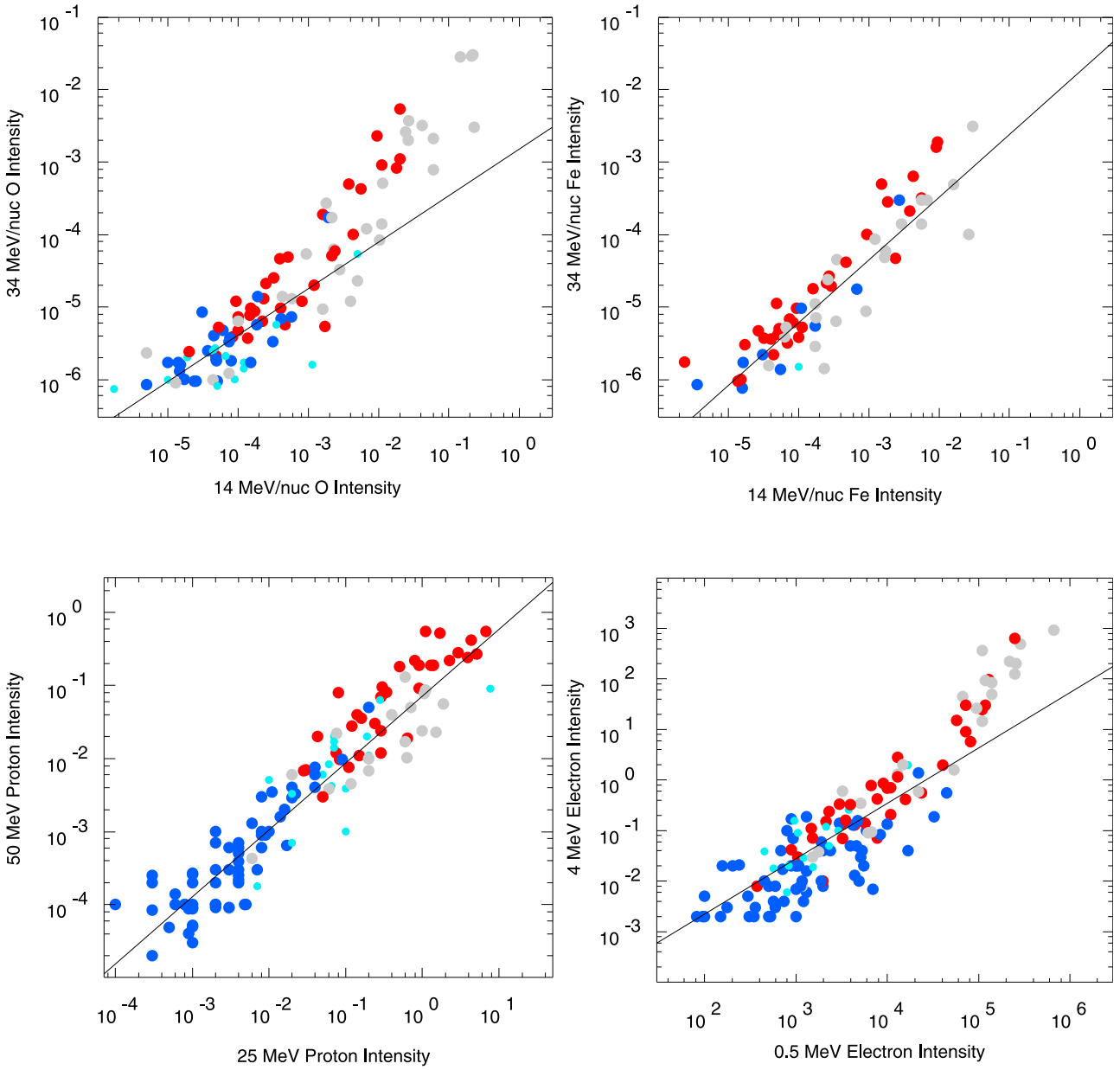

Figure 8. Higher energy intensities [particles/(cm^2 sr s MeV/nucleon)] versus lower energy intensities for protons, electrons, and O and Fe ions with colors indicating group membership. The straight (dark blue) line is fitted to just the group 1 data.

electron–rich. They are defined to be Fe–rich but are not necessarily Fe–rich at 14 MeV/nucleon. (The lower-energy data were used in Figure 7 to increase the number of events on the plot.) Recall also that the distribution of *e*/*p* values does not contain two well–separated groups. Thus, it must be concluded that none of the *e*/*p*, H/He, or Fe/O ratios clearly distinguish a specific set of events from the remaining events along the lines of the simple two-class picture.

4.2. Spectra

[30] Studying detailed spectra is beyond the scope of this study but instead we have examined variations in intensity for a number of energy ranges and species. Figure 8 shows higher energy intensities versus lower energy intensities for protons, electrons, O, and Fe. The plots contain all the events from groups 1–4 and are not restricted in terms of source regions at the Sun. Plotting events only from the 20°–90°W range does not produce significantly different distributions. The straight lines shown are fits to just the group 1 events. For protons (bottom left panel) and Fe (top right panel), all the remaining (groups 2–4) events fall close to this line, suggesting that there is little difference in the proton and Fe spectra, at 25–50 MeV and 14–34 MeV/nucleon respectively, between the different classes of events. For electrons and oxygen, the highest-intensity events tend to lie above the line

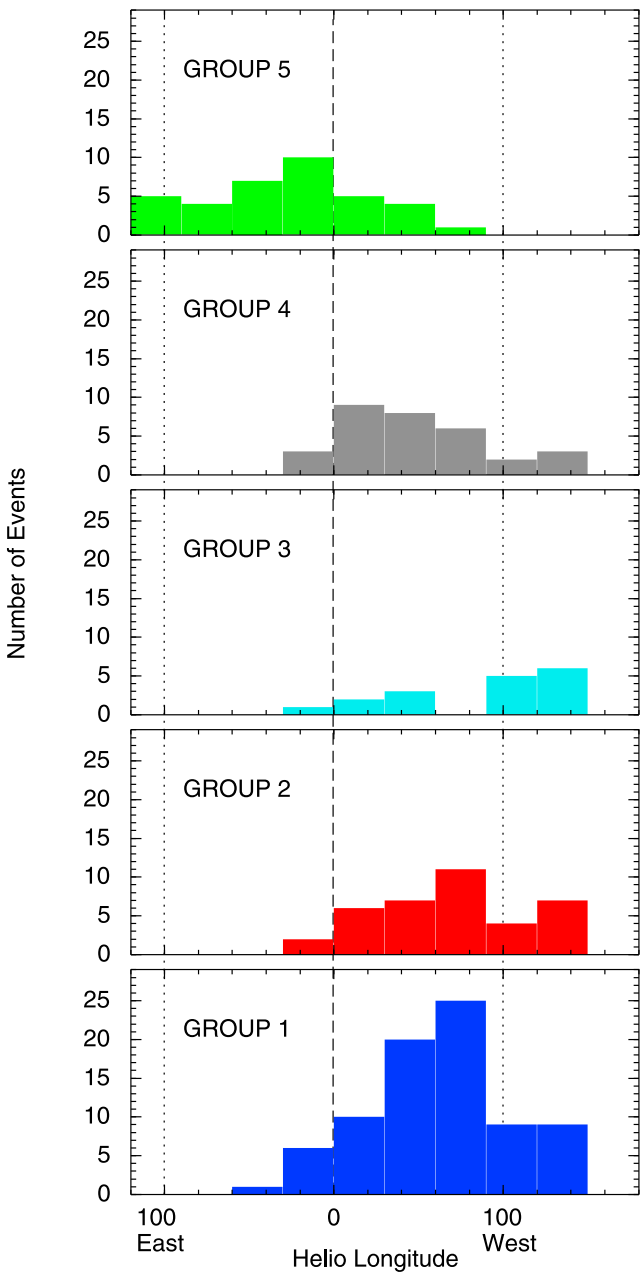

Figure 9. Histograms of event source regions (H α flare longitude for on-disk events) for events in the different groups.

fitted to the group 1 events, implying a hardening of the spectrum, but a more detailed study using full spectral data would be required to verify and investigate this possibility. Probably the most striking aspect of Figure 8 is the transition wherein group 1 events clearly have the lowest proton intensities, to where there is almost complete overlap in the range of Fe intensities for the groups; the distribution for O intensities lies in between.

4.3. Source Regions

[31] Figure 9 shows histograms of the longitudes of the source regions of the 201 events in groups 1 to 5. As might be expected [*Cane et al.*, 1988], the group 5 events with the slowly rising intensities originate primarily in eastern regions, far removed from the foot point of the nominal field line passing near Earth (i.e., 60°W). Note that all other groups (including the group 1, impulsive, events) span very similar longitude ranges extending from just east of the central meridian across the Western Hemisphere to beyond the west limb. However, the distributions within this longitude range are not the same. The Fe-poor group 3 events without in situ shocks mainly originate near and beyond the west limb, whereas the group 4 events, with strong shocks, originate much closer to the central meridian. Note that there are no Fe-poor events without an associated shock (group 3) in the longitude range 60°–90°W.

4.4. CME Properties

[32] Figure 10 shows the early ~25 MeV proton intensities as a function of the angular sizes and speeds of the associated CMEs with event groups identified by color. Note again that all the events in the study, including the group 1 electron-rich events, had associated CMEs. In this figure we included the group 5 events. They are associated with energetic events but have low early proton intensities because of poor magnetic connection to the source region. CMEs with sizes of 360° are omitted because their large size is a projection effect from originating near the central meridian. (Note that this is not true of all the "halo" CMEs reported in the CUA catalog, many of which are associated with highly energetic events originating far from the central meridian. This is one of the reasons why we independently measured the CME sizes, as observed in the C2 coronagraph). It can be seen that group 1 events (dark blue circles) are mainly associated with small CMEs [32 of 69 group 1 events with sizes determined (47%) have sizes <60°]; otherwise there is considerable overlap in the sizes of CMEs associated with events in the different groups. The bottom panel shows that there is also considerable overlap in the speeds of CMEs associated with the different groups. Nevertheless, the group 4 events (gray circles), which have strong shocks, are associated with the fastest CMEs. Overall, as shown by previous workers, the proton intensities increase with increasing CME speed. The correlation improves slightly over that in the figure when only Western Hemisphere, on-disk events are considered.

4.5. Flare Properties

[33] Intensities and durations of the flares associated with the SEP events are shown in Figure 11. We use peak X-ray flare intensities but H α durations. The reason for this is that X-ray intensities are derived from full Sun measurements, unlike H α observations, so X-ray durations may include simultaneous events that cannot be separated. There is considerable overlap in the durations and intensities of flares associated with the events in the different groups, although none of the events for groups 2–5 are associated with flares that lasted less than 26 min. Furthermore, all of the group 4 and 5 events, which have strong shocks, have flares lasting more than 50 min. Considering Western Hemisphere, on-disk events, the correlation between proton intensities and flare intensities is the same as that between proton intensities and CME speeds. For the ~100 events of groups 1–4 originating in the region 60°–90°W, the correlation coefficients are about 0.6.

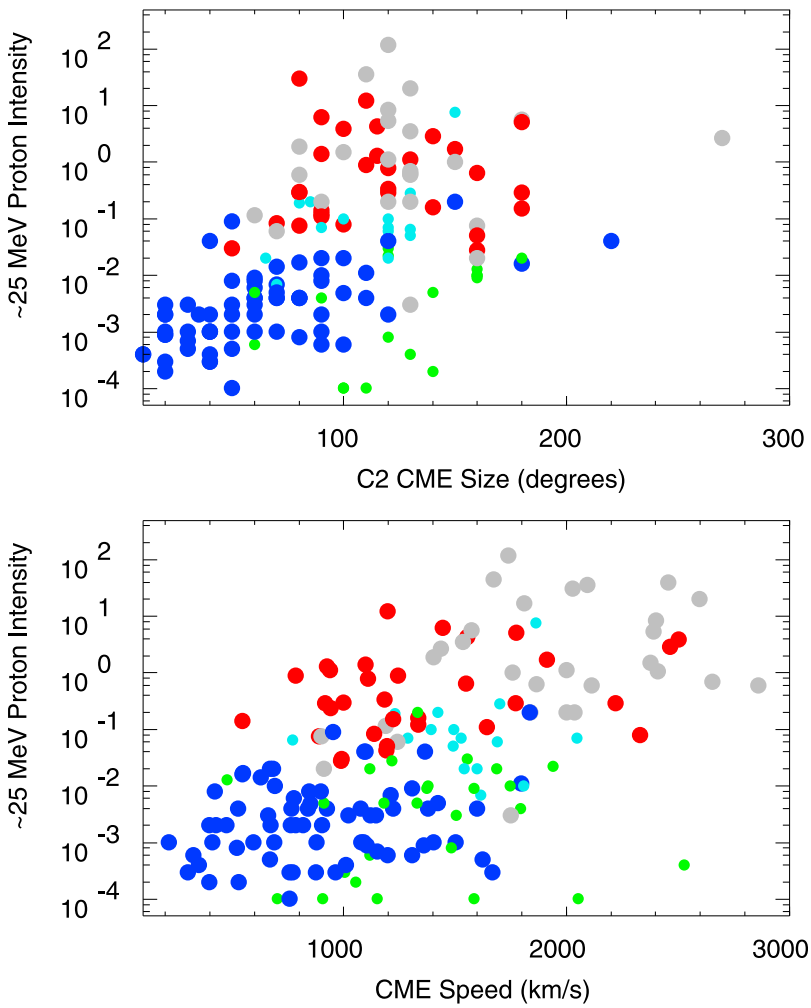

Figure 10. Early ~25 MeV proton intensities as a function of sky-plane speeds and angular sizes for the CMEs associated with events in the different groups.

4.6. Radio Bursts

[34] Figures 12–14 show characteristics of the associated radio bursts. Figure 12 shows histograms of the intensity classes of associated meter-wavelength type II bursts as reported in SGD for events in groups 1, 2, 4, and 5. (Group 3 events had very few events with available radio data and so were omitted from these figures.) We also confirmed that type II bursts were actually present from the dynamic spectra. A zero means no type II burst was reported or that we deemed that one was not present. The color of the histogram indicates the group number. It is clear that metric type II bursts occur for all groups of events and that there is no ordering of intensity by group number.

[35] Figure 13 investigates type III emissions. Of the 280 events listed in Table 1, only two events, both in group 5, had no associated type III emissions. The meter-wavelength dynamic spectra were examined for as many events as possible to determine the timing of the type III emissions relative to the times of soft X-ray and H α maximum intensities. If the type III events were before flare maximum (i.e., they occurred in the flare impulsive phase) then the type III timing was allocated the number 0. If there was also some emission after flare maximum then the number was 1. If there was some emission before flare maximum but the bulk of it was after, then the type III timing number was 2; if all the emission was after flare maximum, the number was 3. We find that the event groups are organized much better by type III emissions than by metric type II emissions. All but one of the events (with available dynamic spectra) with only impulsive-phase type III emissions belonged to group 1 and only one event from group 1 had only late-phase type III emissions.

[36] Figure 14 summarizes the frequency extent and duration of the type II radio emissions seen by Wind/WAVES. If no type II emission was seen then the category was given a 0. Category 1 indicates the presence of emissions that were probable extensions of meter-wavelength type II bursts or were other emissions lasting less than 1 h. Category 2 emissions lasted longer than 1 h but did not extend into kilometer wavelengths. Finally, category 3 indicates the presence of emissions extending to kilometer wavelengths. The majority of the group 4 and 5 events had associated kilometer-wavelength emissions (indicative of the presence of strong interplanetary shocks), whereas only one group 1 event did.

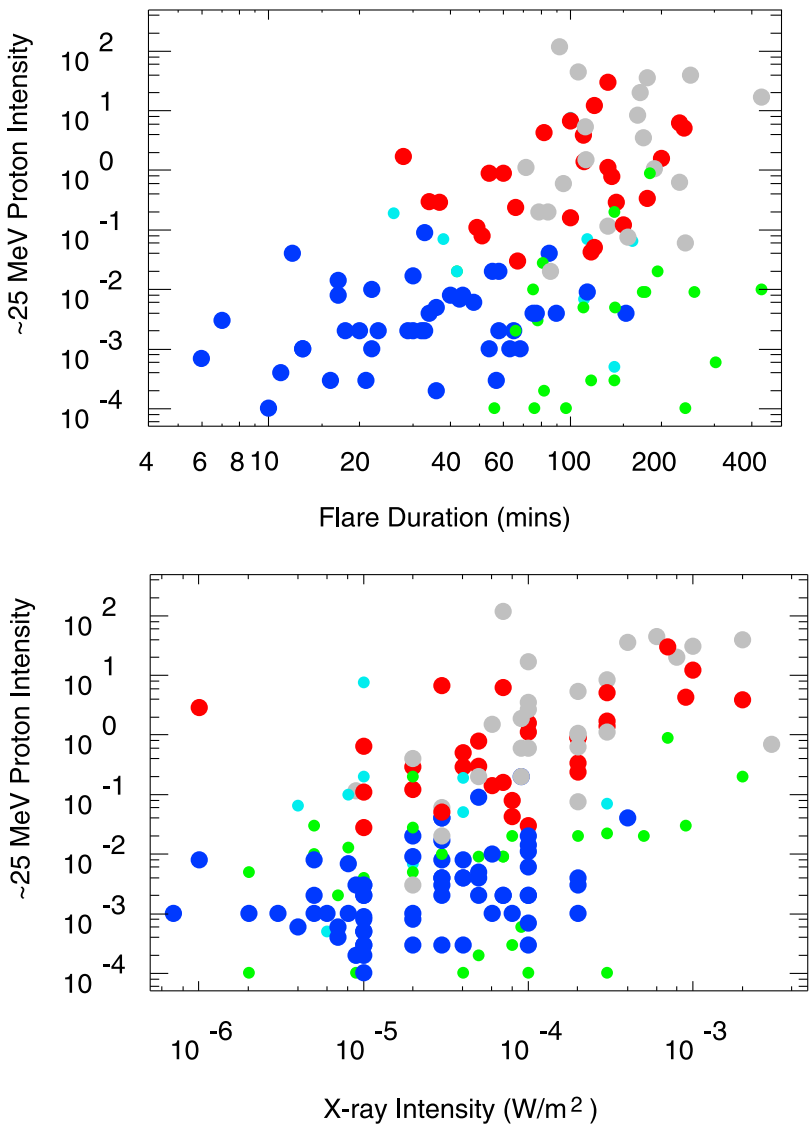

Figure 11. Early ~25 MeV proton intensities as a function of peak soft X-ray intensity and H α flare duration for flares associated with events in the different groups.

Group 2 (and group 3) events that did not have shocks at 1 AU tended not to have associated kilometer-wavelength radio emissions.

5. Discussion and Conclusions

[37] We examined the abundance variations and solar event characteristics in all 280 >25 MeV solar proton events with intensities above 2×10^{-4} particles/(cm^2 sr s MeV) that occurred in 1997–2006. Of these, 201 events were divided into five groups based on the abundances and the particle profiles. The most important result is that there is a continuum of event properties. Although the electron-rich group 1 events, most of which might be judged to be impulsive, are generally also Fe- and He-rich, Figures 1 and 7 show that no clear-cut division of events based on abundances is possible. Group 1 events are also generally associated with smaller CMEs and shorter-duration flares but there are also group 2–5 events that are associated with similar solar events (Figures 10 and 11). With respect to CME speeds and flare peak intensities, there is considerable overlap among the different groups. We should again emphasize that all of our events had associated CMEs. *Kahler* [2001] found that some impulsive events are associated with CMEs but that these were also narrow (10°–40°). In contrast, we found that 54% of our group 1 events (37 out of 69) have sizes greater than 50°. The difference is that our group 1 events are more energetic than the events studied by *Kahler* [2001], who concentrated on events with high ^{3}He/^{4}He ratios; these are the smallest particle events produced by the Sun. Although a number of our group 1 events are in the list of "large" impulsive events of *Reames and Ng* [2004], the majority are not. This is because the *Reames and Ng* [2004] list selects for events with the highest ratios of ^{3}He/^{4}He or Fe/O (at ~2 MeV/nucleon), whereas we started with proton enhancements which have lower ratios for those species [see *Reames et al.*, 1990, Figure 6]. We showed that proton intensities increased as a function of both the flare and the

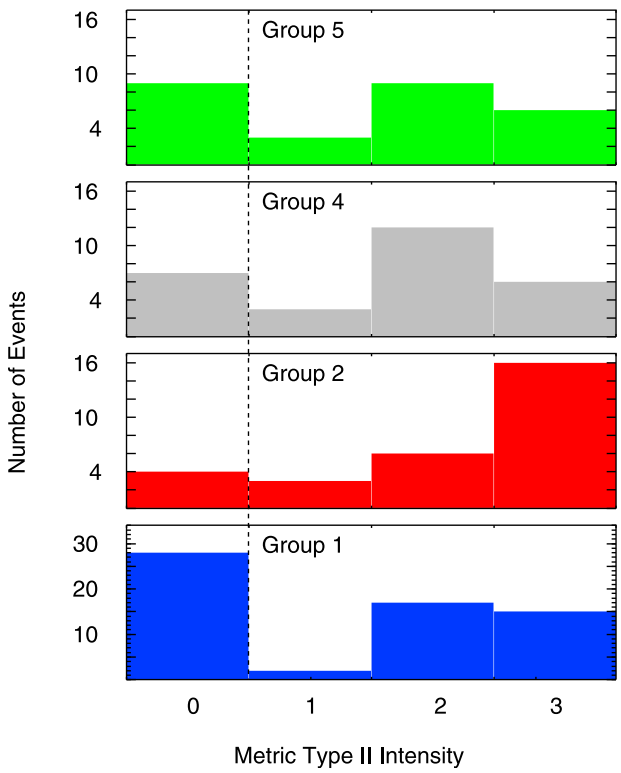

Figure 12. Distribution of metric type II intensities for events in the different groups. Events in bottom panel (blue) belong to group 1. The middle panels are group 2 and 4 events (red and gray), and the top panel is group 5 (green). Group 3 events are not shown because it is a small group. Intensity 0, to the left of the vertical dashed line, indicates no metric type II observed.

CME properties that we examined. That the correlations are all rather similar is not surprising because there is a close physical relationship between flares and CMEs.

[38] If both flares and shocks contribute in large events, as suggested by several authors [e.g., *Kocharov and Torsti*, 2002; *Kallenrode*, 2003; *Cane et al.*, 2006], groups 1 and 2, being electron- and Fe-rich, respectively, would consist primarily of flare particles, whereas the group 4 and 5 events would be primarily composed of shock-accelerated particles. Group 4 (gray) and 5 (green) events had a high incidence of shocks detected at 1 AU and the main difference between them was the flare longitude (Figure 9). Group 5 events, being poorly connected, would be composed solely of shock-accelerated particles. However, in the scenario we propose, the group 5 events would be expected to be group 2 events when viewed from the perspective of a well-connected observer. The group 2 events have a lower incidence of shocks at 1 AU and the shocks were less energetic than those in group 4 based on the lower mean shock transit speed of 804 km/s versus 1140 km/s for events in group 4 and less frequent occurrence of kilometer-wavelength radio emissions. These results are essentially the same as those of *Cane et al.* [2006]; that is, in the presence of strong interplanetary shocks, events have lower Fe/O ratios.

[39] In a previous study [*Cane et al.*, 2006], we started with particle intensity-time profiles and examined abundances, whereas in the present study we started by grouping events using abundances and looked at differences in the associations for these groups of events. We also included much smaller events, which provide the major contributions to groups 1 and 3; compared the intensities of electrons, protons, and He; and compared properties of the associated solar events.

[40] The type III radio observations in Figure 12 support the possibility that flare acceleration is involved in these SEP events. They confirm the result from an earlier study [*Cane et al.*, 2002] that essentially all events have associated type III emissions and that for the largest events these start or extend beyond the maximum of the flare emissions, i.e., after the impulsive phase (see Figure 13). The type III characteristics also provide the strongest correlation found between particle events and solar emissions in that only one group 1 event did not have impulsive-phase/prompt type III emissions and furthermore only one event outside group 1 had only prompt type III emissions. It should be noted that the two electron-rich events that had strong interplanetary shocks and shock-accelerated particles had relatively strong impulsive-phase type III bursts.

[41] These results support and extend those of an earlier study [*Cane et al.*, 2002], in which these "late" type III emissions were called type III-*l*. *Cane et al.* [2002] also

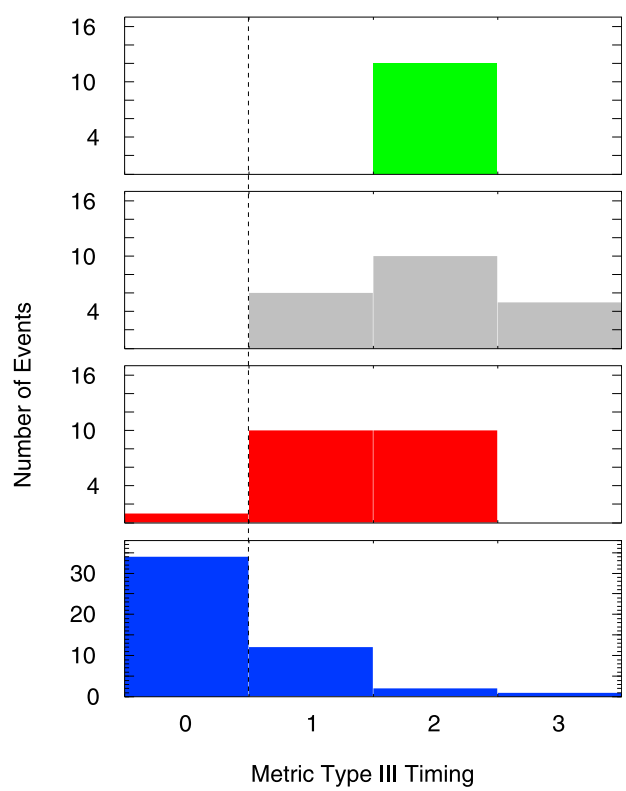

Figure 13. Timing of type III bursts relative to flare emissions for events in different groups. Events to the left of the vertical line had associated type III events that occurred only before maximum flare intensity. Timing 1 indicates there was some type III activity after flare maximum and timing 2 indicates most was after flare maximum. Timing 3 indicates that all type III activity was after flare maximum.

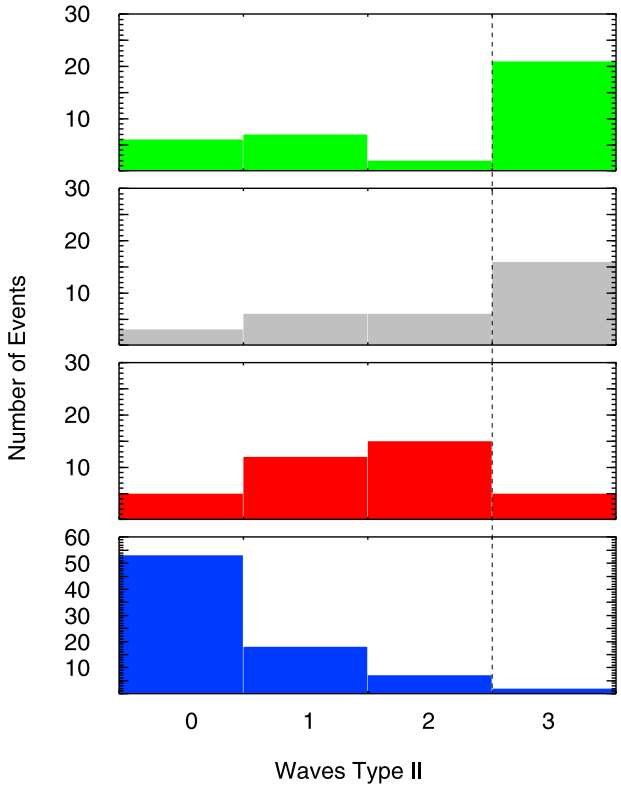

Figure 14. Category of Wind/WAVES type II emission for events in the different groups. Events to the left of the vertical line had either no wave event (category 0), activity that appeared to be a metric type II continuation (category 1), or a short-duration emission not extending to kilometer wavelengths (category 2). Events to the right of the line (category 3) had associated emissions extending to kilometer wavelengths (i.e., interplanetary type II emissions).

performed a reverse study and found that a random sample of type III-*l* bursts were all associated with proton events provided there was reasonable magnetic connection to the spacecraft.

[42] However, we would not necessarily expect "flare particles" in energetic SEP events to have abundances identical to those of impulsive flare events. We reiterate that the term "flare" is used in a broad sense. In energetic SEP events the flare impulsive phase is followed by extended magnetic reconfiguring and particle acceleration, as evidenced by radio imaging [e.g., *Klein and Posner*, 2005; *Maia et al.*, 2007]. This later acceleration is likely to be the same basic process as in the impulsive phase but in an environment with different physical properties. *Petrosian and Liu* [2004] suggested that proton acceleration might be more efficient in the later phases of flares because of a higher gas density in the coronal flare loops. In addition, *Emslie et al.* [2004] found that the *e*/*p* ratio varies inversely with the size of a flare loop and that flare loop sizes increase as flares progress. For "long-duration" γ-ray flares, the proton-to-electron ratio increases after the flare impulsive phase [*Ryan*, 2000]. Thus, the *e*/*p* ratio of a flare-accelerated component in major SEP events is likely to be less than the ratio characterizing small impulsive flare events. As for the Fe/O ratios, they are observed in small events to be larger for shorter-duration flares [*Reames et al.*, 1990], so even though enhanced in large flares (i.e., above values of ~0.1 found in the corona and solar wind) they are unlikely to reach the high values (>10) seen in particles from very small flares. Although it is possible that late phase accelerations occur at coronal shocks, this seems unlikely because radio observations indicate that they occur too low in the corona [e.g., *Klein and Posner*, 2005].

[43] We note that *Cliver and Ling* [2007, 2009] challenged our proposal of an important role for flares in large events. In their first paper, *Cliver and Ling* [2007] looked at *e*/*p* ratios and electron and proton spectra, using observations at two energies. Their *e*/*p* values are different from ours because they used different proton data but they did not demonstrate a bimodal distribution. To provide proton spectral information, *Cliver and Ling* [2007] compared integral proton intensities at >10 and >30 MeV. We note, however, that these are not independent values and, as a result, their correlation plots of the intensities at the two energies show much less scatter than ours. Also they did not find a single distribution as we do and concluded that the more intense events had relatively more high-energy particles because they had inferred flatter spectra than the smaller events. However, if one examines actual proton spectra (i.e., intensities at many energies) published by previous workers [*Reames*, 2000, and references therein] it may be seen that the spectra are flatter because of reduced intensities at low energies. We do not find this change in spectra between small and large events because we use intensities at higher energies. *Cliver and Ling* [2007] also claim that flare particles can only be seen from a very restricted longitude range. However, this finding disagrees with the multispacecraft observations of *Wibberenz and Cane* [2006] and with the longitude extent for sources of group 1 events versus those for group 2–4 events. In their second paper, *Cliver and Ling* [2009] looked at long-lasting type III bursts and disputed our result, obtained earlier and substantiated in the present paper, that a special class of type III emission accompanies major proton events. However, *Cliver and Ling* [2009] failed to take account of the timing of the type III emission relative to the flare emissions. Their comparison of radio intensities and proton intensities takes no account of the fact that they compare inferred total electron intensities relatively close to the Sun with observations at 1 AU, where only a part of the particle beam would be intercepted.

[44] Finally, we address the proposal by *Tylka et al.* [2005] that enhanced Fe/O ratios in a SEP event may be produced by acceleration at a quasi-perpendicular shock of a remnant suprathermal Fe-rich ion population from previous small flare events; in this scenario, particles accelerated in the associated flare play no role. We first of all note that the presence of type III radio emission in all but two of these SEP events (both in group 5) implies that particles accelerated in the concomitant flare can escape into the interplanetary medium. There is therefore no need to invoke a "hypothetical" remnant population from unrelated flares as a source population for shock acceleration. Furthermore, it is difficult to test whether quasi-perpendicular shocks are involved because the configuration of CME shocks near the Sun is not currently known. *Tylka et al.* [2005] suggested that perpendicular shocks are likely to occur on the flanks of CMEs. This might suggest that events in which connection

is to the flank of the shock, rather than to the nose where the shock is likely to be quasi-parallel, would be more likely to be Fe-rich. Thus, we might expect events originating beyond the west limb of the Sun, or from the central meridian or farther east, to be more likely to be Fe-rich than those originating in the well-connected region near ~60°W. However, our observations suggest the opposite: that the Fe-rich events originate near 60°W. This longitude region is where one would expect the most significant flare contribution to occur.

[45] It is also unclear whether quasi-perpendicular shocks produce an Fe-rich accelerated ion population in the presence of an Fe-rich seed population. *Cane et al.* [2007] showed 1 AU data for a shock passing through an Fe-rich flare population. The shock-associated "spike" enhancement, indicating a perpendicular shock, was not Fe-rich.

[46] The solar event properties discussed in this paper cannot be used to infer remnant populations or the configuration of CME-driven shocks near the Sun. Thus, we cannot make a test of the viability of the model by *Tylka et al.* [2005] with this data set apart from the aforementioned aspect of the longitude distribution of Fe-rich and Fe-poor events. On the other hand, we believe that the various data sets we considered do support our model of a flare contribution in major events along with particles accelerated at the associated CME-driven shock.

[47] **Acknowledgments.** We appreciate the use of the data made available via the NSSDC CDAWeb and the ACE data center. We also acknowledge the hard work of the Principal Investogators of the various instruments: R. E. McGuire (IMP 8), J. Torsti (ERNE), R. Müller-Mellin (EPHIN), R. E. Gold (EPAM), G. M. Mason (ULEIS) R. A. Mewaldt (SIS), M. L. Kaiser (WAVES) and, R. A. Howard (LASCO). The CME catalog is generated and maintained at the CDAW Data Center by NASA and The Catholic University of America in cooperation with the Naval Research Laboratory.

[48] Amitava Bhattacharjee thanks the reviewers for their assistance in evaluating this manuscript.

References

Cane, H. V., and W. C. Erickson (2003), Energetic particle propagation in the inner heliosphere as deduced from low-frequency (<100 kHz) observations of type III radio bursts, *J. Geophys. Res.*, *108*(A5), 1203, doi:10.1029/2002JA009488.

Cane, H. V., and W. C. Erickson (2005), Solar type II radio bursts and IP type II events, *Astrophys. J.*, *623*, 1180.

Cane, H. V., R. E. McGuire, and T. T. von Rosenvinge (1986), Two classes of solar energetic particle events associated with impulsive and long-duration soft X-ray flares, *Astrophys. J.*, *301*, 448.

Cane, H. V., D. V. Reames, and T. T. von Rosenvinge (1988), The role of interplanetary shocks in the longitude distribution of solar energetic particles, *J. Geophys. Res.*, *93*, 9555.

Cane, H. V., W. C. Erickson, and N. P. Prestage, (2002), Solar flares, type III radio bursts, coronal mass ejections, and energetic particles, *J. Geophys. Res.*, *107*(A10), 1315, doi:10.1029/2001JA000320.

Cane, H. V., T. T. von Rosenvinge, C. M. S. Cohen, and R. A. Mewaldt (2003), Two components in major solar particle events, *Geophys. Res. Lett.*, *30*(12), 8017, doi:10.1029/2002GL016580.

Cane, H. V., R. A. Mewaldt, C. M. S. Cohen, and T. T. von Rosenvinge (2006), Role of flares and shocks in determining solar energetic particle abundances, *J. Geophys. Res.*, A06S90, doi:10.1029/2005JA011071.

Cane, H. V., I. G. Richardson, and T. T. von Rosenvinge (2007), Fe/O ratios in interplanetary shock accelerated particles, *Space Sci. Rev.*, *130*, 301.

Cliver, E. W., and A. G. Ling (2007), Electrons and protons in solar energetic particle events, *Astrophys. J.*, *658*, 1439.

Cliver, E. W., and A. G. Ling (2009), Low-frequency type III bursts and solar energetic particle events, *Astrophys. J.*, *690*, 598.

Cohen, C. M. S., R. A. Mewaldt, R. A. Leske, A. C. Cummings, E. C. Stone, M. E. Wiedenbeck, E. R. Christian, and T. T. von Rosenvinge (1999), New observations of heavy-ion-rich solar particle events from ACE, *Geophys. Res. Lett.*, *26*(17), 2697.

Emslie, A. G., J. A. Miller, and J. C. Brown (2004), An explanation for the different locations of electron and ion acceleration in solar flares, *Astrophys. J.*, *602*, L69.

Kahler, S. W. (2001), Coronal mass ejections associated with impulsive solar energetic particle events, *Astrophys. J.*, *562*, 558.

Kallenrode, M.-B. (2003), Current views on impulsive and gradual solar energetic particle events, *J. Phys. G: Nucl. Part. Phys.*, *29*, 965.

Klein, K.-L., and A. Posner (2005), The onset of solar energetic particle events: Prompt release of deka-MeV protons and associated coronal activity, *Astron. Astrophys.*, *438*, 1029.

Kocharov, L., and J. Torsti (2002), Hybrid solar energetic particle events observed on board SOHO, *Solar Phys.*, *207*, 149.

Maia, D. J. F., R. Gama, C. Mercier, M. Pick, A. Kerdraon, and M. Karlický (2007), The radio-coronal mass ejection event on 2001 April 15, *Astrophys. J.*, *660*, 874.

Mason, G. M., J. E. Mazur, and J. R. Dwyer (1999), ^{3}He enhancements in large solar energetic particle events, *Astrophys. J.*, *525*, L133.

McGuire, R. E., T. T. von Rosenvinge, and F. B. McDonald (1986), The composition of solar energetic particles, *Astrophys. J.*, *301*, 938.

Nitta, N. V., et al. (2006), Solar sources of impulsive solar energetic particle events and their magnetic field connection to the Earth, *Astrophys. J.*, *650*, 438.

Petrosian, V., and S. Liu (2004), Stochastic acceleration of electrons and protons. I. Acceleration by parallel-propagating waves, *Astrophys. J.*, *610*, 550.

Reames, D. V. (1988), Bimodal abundances in the energetic particles of solar and interplanetary origin, *Astrophys. J.*, *330*, L71.

Reames, D. V. (1995), Solar energetic particles: A paradigm shift, *Rev. Geophys.*, *33*(S1), 585.

Reames, D. V. (1999), Particle acceleration at the sun and in the heliosphere, *Space Sci. Rev.*, *90*, 413.

Reames, D. V. (2000), The observational consequences of proton-generated waves at shocks, in *Acceleration and Transport of Energetic Particles Observed in the Heliosphere*, edited by R. A. Mewaldt et al., *AIP Conf. Proc.*, *528*, 79.

Reames, D. V., and C. K. Ng (2004), Heavy-element abundances in solar energetic particle events, *Astrophys. J.*, *610*, 510.

Reames, D. V., H. V. Cane, and T. T. von Rosenvinge (1990), Energetic particle abundances in solar electron events, *Astrophys. J.*, *357*, 259.

Ryan, J. M. (2000), Long-duration solar gamma-ray flares, *Space Sci. Rev.*, *93*, 581.

Tylka, A. J., et al. (2005), Shock geometry, seed populations, and the origin of variable elemental composition at high energies in large gradual solar particle events, *Astrophys. J.*, *625*, 474.

von Steiger, R. N., N. A. Schwadron, L. A. Fisk, J. Geiss, G. Gloeckler, S. Hefti, B. Wilken, R. R. Wimmer-Schweingruber, and T. H. Zurbuchen (2000), Composition of quasi-stationary solar wind flows from Ulysses Solar Wind Ion Composition Spectrometer, *J. Geophys. Res.*, *105*(A12), 27,217.

Wibberenz, G., and H. V. Cane (2006), Multi-spacecraft observations of solar flare particles in the inner heliosphere, *Astrophys. J.*, *650*, 1199.

Yashiro, S., N. Gopalswamy, G. Michalek, O. C. St. Cyr, S. P. Plunkett, N. B. Rich, and R. A. Howard (2004), A catalog of white light coronal mass ejections observed by the SOHO spacecraft, *J. Geophys. Res.*, *109*, A07105, doi:10.1029/2003JA010282.

H. V. Cane, I. G. Richardson, and T. T. von Rosenvinge, Astroparticle Physics Laboratory, Code 661, NASA Goddard Space Flight Center, Greenbelt, MD 20771, USA. (Hilary.Cane@utas.edu.au; Ian.G.Richardson@nasa.gov; Tycho.T.vonRosenvinge@nasa.gov)